

# Anatomy of Diluted Dark Matter in the Minimal Left-Right Symmetric Model

Miha Nemevšek<sup>1,2,\*</sup> and Yue Zhang<sup>3,†</sup>

<sup>1</sup>*Jožef Stefan Institute, Jamova 39, 1000 Ljubljana, Slovenia*

<sup>2</sup>*Faculty of Mathematics and Physics, University of Ljubljana, Jadranska 19, 1000 Ljubljana, Slovenia*

<sup>3</sup>*Department of Physics, Carleton University, Ottawa, ON K1S 5B6, Canada*

(Dated: December 4, 2023)

## Abstract

Temporary matter domination and late entropy dilution, injected by a “long-lived” particle in the early universe, serves as a standard mechanism for yielding the correct dark matter relic density. We recently pointed out the cosmological significance of diluting particle’s partial decay into dark matter. When repopulated in such a way, dark matter carries higher momentum than its thermal counterpart, resulting in a suppression of the linear matter power spectrum that is constrained by the large scale structure observations. In this work, we study the impact of such constraints on the minimal left-right symmetric model that accounts for the origin of neutrino mass. We map out a systematic anatomy of possible dilution scenarios with viable parameter spaces, allowed by cosmology and various astrophysical and terrestrial constraints. We show that to accommodate the observed dark matter relic abundance the spontaneous left-right symmetry breaking scale must be above PeV and cosmology will continue to provide the most sensitive probes of it. In case the dilutor is one of the heavier right-handed neutrinos, it can be much lighter and lie near the electroweak scale.

---

\* [miha.nemevsek@ijs.si](mailto:miha.nemevsek@ijs.si)

† [yzhang@physics.carleton.ca](mailto:yzhang@physics.carleton.ca)

# CONTENTS

I. Introduction	3
II. Dark matter in the minimal left-right symmetric model	6
A. The minimal left-right symmetric model	6
B. Essential model ingredients for the early universe	8
1. Right-handed currents	8
2. Lightest right-handed neutrino as dark matter	9
3. Neutrino mass contributions	10
4. $W - W_R$ gauge boson mixing	11
5. The Majorana Higgs	12
III. General Dilution mechanism vs. large scale structure	13
A. Relativistic freeze out and overproduction problem	13
B. Entropy dilution mechanism with a long-lived particle	14
C. Dilutor to dark matter decay	15
D. Phase space distribution of dark matter	17
E. Imprint on the matter power spectrum	22
IV. Anatomy of dilution scenarios in LRSM	24
A. Heavy neutrino dilutor	25
1. Implication of the SDSS constraint	25
2. A no-go theorem	26
3. Type-II seesaw dominance and dilutor decay via $N - \nu$ mixing	28
4. Dilutor decay via $W - W_R$ mixing and $X$ -ray limits	30
5. Lower bound on the $W_R$ mass scale	33
B. Majorana Higgs dilutor	34
V. Conclusion and Outlook	38
Acknowledgements	40
A. Radiative $N_1$ decay via $W - W_R$ mixing	40

## I. INTRODUCTION

The field of particle physics and cosmology is facing at least three unresolved issues, driven by experiments: the nature of dark matter, the origin of neutrino mass, and the origin of the matter-anti-matter asymmetry in the universe. They are likely linked to new fundamental laws of nature. Conceptually, it would be very appealing to have these puzzles solved within a single unified framework.

A heavy neutrino is one of the oldest, simplest and most obvious of dark matter candidates. It was first introduced as a Standard Model (SM) gauge singlet with a small mixing with the active neutrinos, produced via active-sterile neutrino oscillations in the early universe. With improved astrophysical observations, both the Dodelson-Widrow [1] and the Shi-Fuller [2] mechanisms are already excluded [3, 4]. To save such oscillation mechanisms, one must resort to novel neutrino self-interactions [5–8]. A common assumption here is a vanishing dark matter population at very early times, which can easily be affected by high-scale new physics. Right-handed neutrinos are often mandatory for gauge anomaly cancellation in many extensions of the SM [9–11]. Assuming the universe was once sufficiently hot, new gauge interactions can then bring them into thermal equilibrium with the SM. A right-handed neutrino can be made cosmologically stable and comprise 100% of dark matter in the universe. While it appears nearly sterile at low energies, the origin of dark matter (its abundance and momentum distribution) is governed by details of the high-scale theory.

The minimal left-right symmetric model (LRSM), based on  $SU(3)_c \times SU(2)_L \times SU(2)_R \times U(1)_{B-L}$  [12–14], was originally proposed as a theory for non-zero neutrino mass [11]. In the model, parity is implemented as a left-right  $Z_2$  symmetry, acting between left- and right-handed fermions. Since  $SU(2)_R$  is gauged, three generations of right-handed neutrinos need to be present to cancel the anomalies. Parity and new gauge symmetries are spontaneously broken above the electroweak scale and light neutrino masses originate from both type-I and II seesaw [11].

Remarkably enough, the Dirac couplings also get predicted [15], which makes the LRSM a particularly complete and predictive theory for neutrino masses. The breaking of lepton

number manifests itself in a number of processes, ranging from direct production at high energy colliders [16, 17], neutrino-less double beta decay [18, 19], LFV [20, 21] and cosmology [22, 23]. Moreover, the model can explain the origin of cosmic baryon asymmetry via leptogenesis, as long as the LR scale is sufficiently high [24, 25].

The lightest right-handed neutrino (called  $N_1$  hereafter) as a viable dark matter candidate in the minimal LRSM was first considered by Bezrukov, Hettmansperger and Lindner [26]. It features a dark matter candidate with a light mass below  $\sim \text{MeV}$ , in order to be cosmologically stable. On the other hand, its mass is bounded from below by several keV scale from phase space packing in dwarf galaxies, because  $N_1$  is a fermion and subject to Pauli blocking [27, 28]. Slightly stronger mass lower bound applies if  $N_1$  had thermal contact with the SM plasma in the early universe (warm dark matter) [3, 29–34]. The right-handed current gauge interaction, mediated by the  $W_R$ , decouples in the early universe and always leaves  $N_1$  freezing out ultra relativistically. This overproduces the dark matter relic abundance, unless there is a “long-lived” matter component that temporarily dominates the energy density of the universe before decaying dominantly into the SM [35]. The late entropy release causes a relative dilution of the final dark matter abundance and brings it down to the observed value. In [26], it was suggested that the role of the diluting particle can be taken on within the LRSM by one of the heavier right-handed neutrinos. The corresponding  $W_R$  boson mass scale is typically constrained to be rather high to facilitate the relativistic freeze-out and longevity of the diluting particle. The possibility of having a lighter  $W_R$  boson was investigated in [36], which resorts to a decaying phase space suppression to keep the lifetime of the diluting particle sufficiently long.

Recently, the dark matter dilution mechanism was revisited and a new, model-independent constraint has been discovered [37]. This new opportunity for testing dark matter dynamics lies in the partial decay of the dilutor into dark matter. Such decay modes exist quite generically, either at tree or loop level, and the branching ratio is sometimes fixed by the internal structure of a UV complete model. With dark matter re-populated this way, the relic density obtains a secondary component on top of the primary one that comes from the usual freeze-out. Most importantly, this component is predicted to be much more energetic than the original thermal one.

Under a reasonable assumption that both the dark matter and the dilutor freeze-out

relativistically<sup>1</sup>, the secondary dark matter particles stay relativistic until the temperature of the universe cools down to around eV scale. This temperature is nearly independent of parameters including the dark matter mass and the dilutor’s mass and lifetime. As a result, dark matter free-streaming strongly impacts the matter power spectrum and the formation of large scale structures. Using the existing data from the Sloan Digital Sky Survey (SDSS), an upper bound on the branching ratio for dilutor into dark matter is set at about  $\lesssim 1\%$ . Because the primordial perturbations remain linear on large scales, a robust cosmological constraint can be applied on the fundamental theories for the origin of dark matter.

In the context of LRSM, the decay of a heavy right-handed neutrino to the lighter one could occur via the exchange of the  $W_R$  gauge boson, similar to weak decays in the SM. If this is the dominant mode, the branching ratio is predicted by the number of lighter fermions and universality of the  $SU(2)_R$  gauge interactions and comes out to be larger than 10%, which turns out to be forbidden by the large scale structure observations [37]. To mitigate this exclusion, the right-handed neutrino dilutor must have other significant decay channels to reduce the dark matter re-population. Such an important constraint has been ignored in previous analysis. We are therefore strongly motivated to revisit the viability of right-handed neutrino dark matter in the LRSM and, as we shall see, they strongly affect the allowed parameter space where an appropriate dark matter relic density can be obtained. In performing a systematic and thorough analysis, we first focus on the usual dilutor in the form of another right-handed neutrino, and then identify a new candidate from the scalar sector of the LRSM that can also play the role of dilution.

Before our journey begins, we would like to stress that the entropy dilution explored here in the context of LRSM is a generic new physics scenario for fixing the dark matter relic density, or for suppressing the amount of extra radiation ( $\Delta N_{\text{eff}}$ ) in the early universe. It has been employed in a broad range of dark matter models including the gravitino, twin-Higgs models, and various dark sector incarnations [38–55]. The same large scale structure constraint would also affect the viability of dark matter in these models and must be taken into account in future studies.

This article is organized as follows. In section II, we give a lightning review of the minimal LRSM and highlight several aspects of the model that are important for the dark matter

<sup>1</sup> We will comment on what happens to the constraint from dilution when this assumption is relaxed. In the LRSM, relativistic freeze-out is always valid, regardless of which particle plays the role of the dilutor.

study in this work. In section III, we discuss the entropy dilution mechanism that features temporary matter domination by a “long-lived” diluting particle. We go beyond the earlier work [37] and provide a detailed derivation of the Boltzmann equation and distribution function of secondary dark matter component from dilutor’s decay. The discussion in this section is model-independent and easily applicable to other models, besides the LRSM, that resort to a similar dilution mechanism. In section IV, we present the anatomy of right-handed neutrino dark matter in the minimal LRSM by exhausting all the possible dilution scenarios that we have envisioned. This includes the heavier right-handed neutrino or the Higgs boson counterpart of left-right symmetry breaking (the right-handed triplet) playing the role of dilutor. For each of the cases, we establish the viable parameter space for DM, compatible with the large scale structure limits from SDSS, along with other constraints that include the correct relic density, generation of neutrino mass, big-bang nucleosynthesis and  $X$ -ray line searches. We also comment on supernova cooling and existing laboratory constraints on the LR scale. We conclude and provide an outlook of opportunities in section V.

## II. DARK MATTER IN THE MINIMAL LEFT-RIGHT SYMMETRIC MODEL

We start with a brief overview of the structure of the minimal LRSM and highlight several ingredients that are important for understanding the cosmology in the later sections. We refer to [12–14] for the original works and in-depth reviews of the model.

### A. The minimal left-right symmetric model

The LRSM is based on the gauge group  $G_{\text{LR}} = SU(3)_c \times SU(2)_L \times SU(2)_R \times U(1)_{B-L}$ , with a discrete  $Z_2$  symmetry interchanging the left and right  $SU(2)$  sectors. At low energies, the  $Z_2$  symmetry manifests itself as the parity symmetry of QCD and QED. Quarks and leptons come in parity symmetric representations

$$\begin{aligned}
 Q_L = \begin{pmatrix} u_L \\ d_L \end{pmatrix} &= \left( 3, 2, 1, \frac{1}{3} \right), & Q_R = \begin{pmatrix} u_R \\ d_R \end{pmatrix} &= \left( 3, 1, 2, \frac{1}{3} \right), \\
 L_L = \begin{pmatrix} \nu \\ \ell_L \end{pmatrix} &= (1, 2, 1, -1), & L_R = \begin{pmatrix} N \\ \ell_R \end{pmatrix} &= (1, 2, 1, -1),
 \end{aligned}
 \tag{2.1}$$

where  $N$  stands for the right-handed neutrino. The scalar potential of the minimal model is also parity symmetric. It consists of three complex fields: a bi-doublet  $\Phi = (1, 2, 2, 0)$  and two triplets  $\Delta_L = (1, 3, 1, 2)$  and  $\Delta_R = (1, 1, 3, 2)$  under  $G_{LR}$ , with the following field assignments

$$\Phi = \begin{pmatrix} \phi_1^0 & \phi_2^+ \\ \phi_1^- & \phi_2^0 \end{pmatrix}, \quad \Delta_{L,R} = \begin{pmatrix} \delta^+/\sqrt{2} & \delta^{++} \\ \delta^0 & -\delta^+/\sqrt{2} \end{pmatrix}_{L,R}. \quad (2.2)$$

Under parity,  $\Phi \rightarrow \Phi^\dagger$ ,  $\Delta_L \leftrightarrow \Delta_R$ . Starting from the LR and parity symmetric potential, it was shown that parity is broken spontaneously [13, 14], with either with two doublets [14] or two triplets [11, 18]. The complete form of the potential was discussed in [56] and studied in some depth in subsequent years [57–61] with more recent works focusing on phenomenological signals [62–64]. A strong lower bound from perturbativity of the potential was worked out in [65], with constraints from vacuum the vacuum structure [66] and opportunities for gravitational waves [67].

The above quantum numbers allow for the following Yukawa terms that couple the fermions to scalars

$$\begin{aligned} \mathcal{L}_{\text{Yuk}} = & \bar{Q}_L \left( Y_q \Phi + \tilde{Y}_q \tilde{\Phi} \right) Q_R + \bar{L}_L \left( Y_l \Phi + \tilde{Y}_l \tilde{\Phi} \right) L_R \\ & + Y_{\Delta_L} L_L^T i\sigma_2 \Delta_L L_L + Y_{\Delta_R} L_R^T i\sigma_2 \Delta_R L_R + \text{h.c.} . \end{aligned} \quad (2.3)$$

where  $\tilde{\Phi} = i\sigma_2 \Phi^* i\sigma_2$  and we suppressed the family indices. The  $\sigma_2$  matrices operate within the two  $SU(2)_{L,R}$  group spaces and ensure gauge invariance. The first two terms are of the Dirac type and give the usual mass terms that connects the left and right chiral fields, as in the SM. A new feature is the Dirac term for neutrinos and the Majorana-type Yukawa couplings  $Y_{\Delta_{L,R}}$  in the second line, that generate lepton number violating masses for neutrinos.

The spontaneous symmetry breaking occurs in two steps. First, the  $SU(2)_R \times U(1)_{B-L}$  symmetry is broken down to  $U(1)_Y$  for hypercharge by the vacuum expectation value (VEV) of the right-handed scalar triplet  $\langle \Delta_R^0 \rangle = v_R/\sqrt{2}$ , which lies well above the electroweak scale. It generates masses for the new gauge bosons  $W_R^\pm$  and  $Z'$ , with a mass relation  $M_{Z'} = \sqrt{3}M_{W_R}$ . Through the  $Y_{\Delta_R}$  Yukawa coupling term in Eq. (2.3), the  $v_R$  condensate also gives a Majorana mass to the right-handed neutrinos  $N$ .

The second stage of spontaneous symmetry breaking is triggered by the VEV of the bi-doublet scalar,  $\langle \phi_1^0 \rangle = v \cos \beta/\sqrt{2}$  and  $\langle \phi_2^0 \rangle = v \sin \beta e^{i\alpha}/\sqrt{2}$ , where  $v = 246$  GeV. Without

loss of generality, we choose  $\beta \in (0, \pi/2)$ . In view of  $SU(2)_L$ , the bi-doublet effectively behaves as two Higgs doublets, thus their VEVs can give masses to the regular  $W^\pm$  and  $Z$  gauge bosons that mediate the weak interactions. Through the Yukawa coupling in Eq. (2.3), the electroweak VEVs also provide Dirac mass matrices for all the fermions, including the one between left-handed neutrinos  $\nu$  and right-handed ones  $N$ .

## B. Essential model ingredients for the early universe

### 1. Right-handed currents

The most important ingredient of the LRSM, relevant for dark matter cosmology, are the new gauge interactions, mediated by the  $W_R^\pm$  and  $Z'$  gauge bosons. The right-handed charged-current interactions for fermions take on the form

$$\mathcal{L}_{\text{gauge}} = \frac{g}{\sqrt{2}} W_R^\mu \left( \bar{N} \gamma_\mu V_{\text{PMNS}}^{R\dagger} \ell_R + \bar{u}_R \gamma_\mu V_{\text{CKM}}^R d_R \right) + \text{h.c.}, \quad (2.4)$$

where all the fermions fields are now in their mass eigenstates. We have introduced the right-handed CKM and PMNS matrices that transform the fermions from the weak flavor into the mass basis. Here we neglected the mixing between the  $W$  and  $W_R$  gauge bosons, which is constrained to be small (see Sec. IIB 4) and its effects in dark matter phenomenology will be accounted for in IVA 4 and A.

In the minimal LRSM with parity symmetry, the right-handed CKM matrix has been solved both numerically [68–70] and analytically [71, 72]. Its off-diagonal elements are suppressed by similar powers of the Wolfenstein parameter as the regular CKM matrix, but all the matrix elements carry extra phase factors with implications for the strong CP violation [70, 73–75]. For the purposes of this work, the exact form of the quark charged currents is not really important and we shall approximate  $V_{\text{CKM}}^R$  with a unit matrix. The situation is quite different for the leptons. There, the form of right-handed PMNS matrix is much less constrained and allowed to be wildly different from the regular PMNS matrix. The only special case is when the light neutrino mass contribution is dominated by the type-II seesaw contribution. In this case, parity requires that  $V_{\text{PMNS}}^R$  be identical to its left-handed counterpart.



2. *Lightest right-handed neutrino as dark matter*

The minimal LRSM does not preserve any exact  $Z_2$  symmetry that would stabilize DM, even LR parity gets broken spontaneously and its quality is not crucial for dark matter stability. As a result, none of the new particles beyond the SM are absolutely stable. As argued in [36], the only candidate for dark matter in the model is the lightest right-handed neutrino,  $N_1$ <sup>2</sup>. Without fine-tuning the flavor structure of  $V_{\text{PMNS}}^R$ , the Feynman diagram in Fig. 1 shows the dominant interaction for  $N_1$  to couple with the charged leptons and quarks.

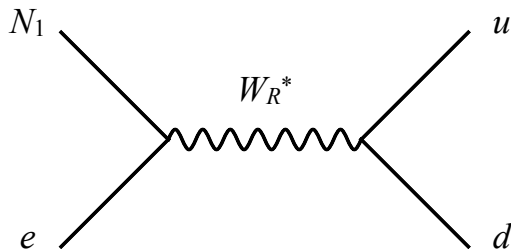


FIG. 1. Feynman diagram for right-handed charged-current interaction of dark matter  $N_1$  in LRSM.

If heavy enough,  $N_1$  could decay into an electron and a charged pion, and it would not be cosmologically stable, unless the  $W_R$  boson is ultra heavy, near the GUT scale<sup>3</sup>. In this work, we are interested in finding lower (and upper) bounds of  $W_R$ , and we will focus on the  $N_1$  dark matter mass below  $\sim 100$  MeV, where there is a wide portion of parameter space for  $N_1$  to be sufficiently stable. To be more specific, the upper bound on  $N_1$  mass can be written as

$$m_{N_1} < \max \left( \left( \frac{96\pi^3}{\tau G_F^2} \right)^{1/5} \left( \frac{M_{W_R}}{M_W} \right)^{4/5}, m_\pi \right) \simeq m_\pi \times \max \left( \left( \frac{M_{W_R}}{10^{10} \text{GeV}} \right)^{4/5}, 1 \right), \quad (2.5)$$

where we require dark matter decay rate  $\tau^{-1} \lesssim 10^{-50}$  GeV, which corresponds to a typical bound from cosmic ray positrons and X-ray searches. As for laboratory constraints, the mass of the  $W_R$  boson is chiefly bounded by searches at the Large Hadron Collider (LHC). For RH neutrinos below a few 10 of GeV, the signal from  $W_R \rightarrow \ell N_1$  looks like a very energetic charged lepton and missing energy, because  $N_1$  escapes detection. Recasting the

<sup>2</sup> The real part of  $\Delta_R^0$  in (2.2) may also be cosmologically stable if it is made to be much lighter than  $M_{W_R}$ . This brings in issues with vacuum stability, similar to the case of the SM [76, 77], and may require fine-tuning of couplings in the LRSM [65, 78, 79], therefore we do not pursue this option any further.

<sup>3</sup> One may consider the PMNS coupling of  $N_1$  to  $\tau$  only, which would prevent the tree-level decay to  $e\pi$  and allow for slightly heavier  $N_1$ .

generic  $W' \rightarrow \ell \bar{\nu}$  searches [80], the current bounds set the LR scale to be  $M_{W_R} \gtrsim 5 \text{ TeV}$ , depending on the flavor of the charged lepton. This channel is particularly clean and may probe the scales up to 37 TeV at a future 100 TeV collider [81].

With such super-weak interactions, mediated by the Feynman diagram in Fig. 1, the RH neutrinos thermalize in the early universe and decouple at temperatures

$$T_d \sim 1 \text{ MeV} \left( \frac{M_{W_R}}{M_W} \right)^{4/3} \gtrsim 300 \text{ MeV}, \quad (2.6)$$

where in the second step we apply the existing lower bound on  $M_{W_R}$  from the LHC. Comparing with Eq. (2.5), we find that

$$T_d > m_{N_1}, \quad (2.7)$$

always holds. We will assume that the reheating temperature of the early universe was sufficiently high, such that all the RH neutrinos (and other particles in the LRSM) were once kept in thermal equilibrium by gauge interactions. The above comparison implies that  $N_1$  must decouple when it was still ultra relativistic, similar to the decoupling of SM neutrinos. As will be sharpened in section III A, this leads to a severe dark matter overproduction problem and requires a non-standard cosmology after the freeze out.

### 3. Neutrino mass contributions

Neutrino masses in the minimal LRSM come from two sources. First, the Dirac neutrino mass term together with the Majorana mass for  $N$ , generated by spontaneous symmetry breaking, can give mass to the active neutrinos through the type-I seesaw mechanism. In addition, the model features another contribution through the type-II seesaw. It comes from the VEV of the left-handed scalar triplet  $\langle \Delta_L^0 \rangle = v_L/\sqrt{2}$  and the  $\lambda$  Yukawa coupling term in Eq. (2.3). The  $v_L$  condensate originates from terms in the scalar potential of the form, e.g.,  $\text{Tr}(\Delta_L \Phi \Delta_R \Phi^\dagger)$ , which is a tadpole term for  $\Delta_L$  after  $\Phi$  and  $\Delta_R$  have obtained their condensates.

The full neutrino mass matrix in the model is then given by

$$M_\nu = -M_D^T M_N^{-1} M_D + M_L, \quad M_D = \frac{v}{\sqrt{2}} \left( \cos \beta Y_l + \sin \beta e^{-i\alpha} \tilde{Y}_l \right), \quad (2.8)$$

$$M_N = \frac{v_R}{\sqrt{2}} Y_{\Delta_R}, \quad M_L = \frac{v_L}{\sqrt{2}} Y_{\Delta_L}. \quad (2.9)$$

Accommodating the neutrino masses and mixings, needed to explain neutrino masses and fit the neutrino oscillations, is one of the primary motivations for considering the LRSM as a plausible BSM theory. We will use it as an important guiding principle when exploring cosmological aspects of the model.

#### 4. $W - W_R$ gauge boson mixing

Because the scalar bidoublet  $\Phi$  transforms under both  $SU(2)_L$  and  $SU(2)_R$ , its VEVs allow for a mixing between the  $W$  and  $W_R$  gauge bosons. The corresponding mass terms take on the form

$$\mathcal{L}_W = - \begin{pmatrix} A_{L\mu}^- & A_{R\mu}^- \end{pmatrix} \frac{g^2}{2} \begin{pmatrix} \frac{1}{2}(v^2 + 2v_L^2) & -v^2 \sin \beta \cos \beta e^{-i\alpha} \\ -v^2 \sin \beta \cos \beta e^{i\alpha} & \frac{1}{2}(v^2 + 2v_R^2) \end{pmatrix} \begin{pmatrix} A_L^{\mu+} \\ A_R^{\mu+} \end{pmatrix}, \quad (2.10)$$

where  $A_{L,R}^\pm$  are the gauge bosons in the flavor basis. After diagonalization, the mass eigenstates are the SM-like  $W$  boson, which is a linear superposition of mostly  $A_L$  and a small admixture of  $A_R$  that mediates RH currents. Vice-versa, the  $W_R$  mass eigenstate is mostly right-handed. Phenomenologically, the relevant scales in the LRSM need to be hierarchical, such that  $v_R \gg v \gg v_L$  and the  $W - W_R$  mixing is approximated by

$$\xi_{LR} \simeq \sin \beta \cos \beta e^{i\alpha} \left( \frac{v}{v_R} \right)^2 \simeq \sin(2\beta) e^{i\alpha} \left( \frac{M_W}{M_{W_R}} \right)^2, \quad (2.11)$$

where in the last step we used  $M_W^2 \simeq g^2 v^2 / 4$  and  $M_{W_R}^2 \simeq g^2 v_R^2 / 2$ . As we will see,  $\xi_{LR}$  is one of the key LRSM parameters for resolving the dark matter re-population issue.

Clearly  $\xi_{LR}$  is suppressed due to the small mass ratio  $(M_W/M_{W_R})^2$ . The magnitude of  $\xi_{LR}$  also depends on  $\tan \beta$ , i.e. the ratio of the two VEVs from the bi-doublet for which there exist an upper bound from the perturbativity of Yukawa couplings. To make the point, we consider the quark mass generation in the minimal LRSM here and explain the logic by approximating with the third family only, which has the largest Yukawa couplings. For a single generation, the top and bottom quark masses are given by

$$m_t = \frac{v}{\sqrt{2}} \left( Y_q \cos \beta + \tilde{Y}_q \sin \beta e^{-i\alpha} \right), \quad m_b = \frac{v}{\sqrt{2}} \left( Y_q \sin \beta e^{i\alpha} + \tilde{Y}_q \cos \beta \right). \quad (2.12)$$

These can be inverted and solved for the Yukawa couplings

$$Y_q e^{i\alpha} = \frac{\sqrt{2}}{v \cos 2\beta} (m_t e^{i\alpha} \cos \beta - m_b \sin \beta), \quad \tilde{Y}_q = \frac{\sqrt{2}}{v \cos 2\beta} (-m_t e^{i\alpha} \sin \beta + m_b \cos \beta). \quad (2.13)$$

By requiring  $|Y_q|$  and  $|\tilde{Y}_q|$  to take on perturbative values ( $\lesssim 3$ ) for  $\alpha \in [0, 2\pi)$ , we get the following allowed range for  $\tan \beta$

$$\tan \beta < -1.24 \quad \cup \quad -0.77 < \tan \beta < 0.77 \quad \cup \quad \tan \beta > 1.24. \quad (2.14)$$

In other words, the large difference between the top and bottom quark masses forbids the angle  $\beta$  to be close to  $\pm\pi/4$ , where  $\cos 2\beta$  approaches to zero blowing up  $Y_q$  and  $\tilde{Y}_q$ . See [70] for more details and a full numerical study with three generations.

### 5. The Majorana Higgs

As mentioned earlier, the gauge symmetry breaking from LRSM to the SM is triggered by the VEV of the  $SU(2)_R$  scalar triplet  $\Delta_R$ . Its components  $\delta_R^\pm$ , and the imaginary part of  $\delta_R^0$ , become the longitudinal components of the  $W_R^\pm$  and  $Z'$  bosons, respectively. The real part of  $\delta_R^0$  is the ‘‘Higgs boson’’ for this step of symmetry breaking, a massive propagating particle that reveals the nature of spontaneous breaking. We denote the properly normalized physical state as  $\Delta$ , where

$$\Delta \equiv \sqrt{2}\delta_R^0 - v_R. \quad (2.15)$$

Because  $v_R$  violates lepton number and serves as the source of Majorana neutrino mass,  $\Delta$  is referred to as the Majorana Higgs [79]. The doubly charged component  $\Delta_R^{++}$  is left over as another physical state.

As will be discussed section IV B,  $\Delta$  can also play a crucial role of dilution for addressing the dark matter relic density. Here, we list its interactions that are relevant for understanding its role in the early universe. The  $\Delta$  is the excitation above the VEV  $v_R$ , which is mostly responsible for the mass generation for the right-handed neutrinos  $N$  and  $W_R^\pm$ ,  $Z'$  gauge bosons. The corresponding couplings can be derived by shifting  $v_R \rightarrow v_R(1 + \Delta/v_R)$ ,

$$\mathcal{L} = -\frac{m_N}{v_R} \bar{N} N \Delta + 2 \frac{M_{W_R}^2}{v_R} W_{R\mu}^+ W_R^{-\mu} \Delta + \frac{M_{Z'}^2}{v_R} Z'_\mu Z'^{\mu} \Delta, \quad (2.16)$$

where we keep the interaction terms linear in  $\Delta$ , which are useful for calculating its decay rates. The  $\Delta - N$  coupling is diagonal in the mass basis of  $N$ .

Another important parameter that controls the decay rates of  $\Delta$  is its mixing with the Higgs boson,  $\theta_{\Delta h}$ . In the presence of such mixing,  $\Delta$  can decay into all the SM particles that the Higgs boson couples to. In particular, when the mass of  $\Delta$  is much above the

electroweak scale, it mainly decays into  $W^+W^-$ ,  $ZZ$  and  $hh$ , with a ratio of  $2 : 1 : 1$ , as dictated by the equivalence principle. The scalar potential terms that couple  $\Delta$  to Higgs are  $\alpha_1 \text{Tr}(\Phi^\dagger \Phi) \text{Tr}(\Delta_R^\dagger \Delta_R) + [\alpha_2 \text{Tr}(\Phi^\dagger \tilde{\Phi}) \text{Tr}(\Delta_R^\dagger \Delta_R) + \text{h.c.}] + \alpha_3 \text{Tr}(\Phi^\dagger \Phi \Delta_R^\dagger \Delta_R)$  [59]. After the right-handed triplet  $\Delta_R$  develops the VEV, but before the electroweak symmetry breaking, these terms allow  $\Delta$  to decay into a pair of SM Higgs bosons, as well as the would-be Goldstone bosons that eventually become the longitudinal components of the  $W$  and  $Z$  bosons.

### III. GENERAL DILUTION MECHANISM VS. LARGE SCALE STRUCTURE

We review the dark matter dilution mechanism under the sudden decay approximation [35], which is a useful tool for exploring the late decay of long-lived particles in the early universe. This approximation allows us to analytically derive the important parametrical dependence in relevant quantities, such as the final dark matter relic density  $\Omega_X$ , and the reheating temperature  $T_{\text{RH}}$  immediately after the decay of the dilutor. To keep the discussion here as general as possible, we call here the dark matter particle  $X$  and the cosmologically “long-lived” particle for entropy dilution  $Y$ . We will assign their identities within the LRSM ( $X \rightarrow N_1, Y \rightarrow N_2, \Delta$ ) in the next section, when we discuss the concrete dark matter dilution scenarios.

#### A. Relativistic freeze out and overproduction problem

Consider the dark matter  $X$ , which freezes out from the SM thermal plasma relativistically. The yield  $Y_X = n_X/s$  is then defined as the ratio of number density  $n_X$  to the total entropy density  $s$  of the SM plasma, and is given by

$$Y_X = \frac{135 \zeta(3)}{4\pi^4 g_*(T_{\text{fo}})}, \quad (3.1)$$

where we assumed that  $X$  is a Majorana fermion with 2 degrees of freedom. The  $T_{\text{fo}}$  is the photon temperature when  $X$  freezes out, and  $g_*(T_{\text{fo}})$  counts the corresponding number of relativistic degrees of freedom in the universe in the plasma. Because most of our discussion will be restricted to temperatures above the MeV scale for successful big-bang nucleosynthesis (BBN), we will not distinguish  $g_*(T)$  and  $g_{*S}(T)$  hereafter. If nothing else happened after the freeze out,  $Y_X$  would be a conserved quantity, and the dark matter relic density today

would be

$$\Omega_X^0 = \frac{m_X Y_X s_0}{\rho_0} \simeq 2.6 \left( \frac{m_X}{1 \text{ keV}} \right) \left( \frac{100}{g_*(T_{\text{fo}})} \right), \quad (3.2)$$

where  $s_0 = 2891.2 \text{ cm}^{-3}$  is the entropy density in the universe today, and  $\rho_0 = 1.05 \times 10^{-5} h^2 \text{ GeV/cm}^3$  represents today's critical density with  $h = 0.67$  [82]. In contrast, the *Planck* experiment observes that the value of  $\Omega_{\text{dark matter}}$  is 0.26 [83]. Because  $m_X$  is constrained to be heavier than several keV due to various warm dark matter constraints, the above result creates the dark matter overproduction problem.

### B. Entropy dilution mechanism with a long-lived particle

To address the issue of overproduction, we introduce a dilutor particle  $Y$ . For simplicity, we assume it is also a Majorana fermion that freezes out relativistically and has a similar yield as the dark matter before decaying away, mostly into the SM particles. To achieve sufficient dilution,  $Y$  must dominate the total energy density of the universe (as matter) before it decays away and dumps most of its energy (or entropy) into the SM sector.

In the sudden decay approximation, we have

$$\tau_Y^{-1} = H_{\text{before}} = H_{\text{after}}, \quad (3.3)$$

where  $\tau_Y$  is the lifetime of  $Y$ , and  $H_{\text{before, after}}$  are the Hubble parameters ( $H \equiv \sqrt{8\pi G_N \rho/3}$ ) immediately before and after the decay, respectively.

Before the decay of  $Y$ , the universe is dominated by the energy density of non-relativistic massive  $Y$  particles,

$$\rho = \rho_Y = Y_Y s_{\text{before}} m_Y, \quad (3.4)$$

where  $s_{\text{before}}$  is the total entropy density of relativistic species before the decay. Here we assume that  $Y$  experiences a similar relativistic freeze out as dark matter and  $Y_Y$  is the same as  $Y_X$  given in Eq. (3.1). Note that the universe is already matter dominated right before  $Y$  decays. However, this does not prevent us from defining  $Y$  as the ratio of  $n_Y$  to the relativistic entropy density  $s$ , and  $Y_Y = n_Y/s$  remains conserved in the time window between the freeze-out and  $Y$ 's decay. With these inputs, the first of Eq. (3.3) leads to

$$s_{\text{before}} = \frac{\pi^3 g_*(T_{\text{fo}})}{90\zeta(3)} \frac{M_{\text{pl}}^2}{m_Y \tau_Y^2}. \quad (3.5)$$

Assuming that the decay of  $Y$  takes no time, the energy density of  $Y$  immediately before its decay is equal to the radiation energy density immediately after. The latter is related to the corresponding ‘‘reheating’’ temperature  $T_{\text{RH}}$  of the SM plasma,

$$\rho = \rho_R = \frac{\pi^2}{30} g_*(T_{\text{RH}}) T_{\text{RH}}^4. \quad (3.6)$$

The second equation of Eq. (3.3),  $\tau_Y^{-1} = H_{\text{after}}$ , leads to

$$T_{\text{RH}} \simeq 0.6 g_*(T_{\text{RH}})^{-1/4} \sqrt{\frac{M_{\text{pl}}}{\tau_Y}} \simeq \frac{0.93 \text{ MeV}}{g_*(T_{\text{RH}})^{1/4}} \sqrt{\frac{1 \text{ sec}}{\tau_Y}}, \quad (3.7)$$

where  $M_{\text{pl}} = \sqrt{1/G_N} = 1.2 \times 10^{19} \text{ GeV}$  is the Planck constant. The entropy density of the SM plasma immediately after  $Y$  decay can then be calculated in terms of  $T_{\text{RH}}$ ,

$$s_{\text{after}} = \frac{2\pi^2}{45} g_*(T_{\text{RH}}) T_{\text{RH}}^3. \quad (3.8)$$

With Eqs. (3.5) and (3.8) we can derive the dilution factor  $\mathcal{S}$ ,

$$\mathcal{S} \equiv \frac{s_{\text{after}}}{s_{\text{before}}} \simeq \frac{0.7 g_*(T_{\text{RH}})^{1/4} m_Y \sqrt{\tau_Y}}{g_*(T_{\text{fo}}) \sqrt{M_{\text{pl}}}}. \quad (3.9)$$

The diluted relic density of  $X$  today is given by

$$\begin{aligned} \Omega_X &= \frac{\Omega_X^0}{\mathcal{S}} \simeq \frac{0.72 g_*(T_{\text{RH}})^{1/4} m_Y \sqrt{\tau_Y}}{g_*(T_{\text{fo}}) \sqrt{M_{\text{pl}}}} \\ &\simeq 0.26 \left( \frac{m_X}{1 \text{ keV}} \right) \left( \frac{2.2 \text{ GeV}}{m_Y} \right) \sqrt{\frac{1 \text{ sec}}{\tau_Y}}. \end{aligned} \quad (3.10)$$

This is the standard dark matter dilution mechanism that has been employed in various contexts for addressing the dark matter relic density.

### C. Dilutor to dark matter decay

We recently pointed out [37] new opportunities to test the dark matter dilution mechanism. We showed that the re-population of dark matter in  $Y$  decays leaves an imprint on structure formation, and gets constrained by the existing data (or gives a characteristic signal upcoming data). While in [37] we worked in a largely model independent way, in a concrete UV realization of such mechanisms, the model predicts not only the relic density, but also the spectrum – the phase space distribution of dark matter with a primary and

secondary component. To account for all these possibilities, we consider the following decay channels of  $Y$ , where it can decay into SM particles as well as dark matter  $X$ ,

$$Y \rightarrow SM, \quad Y \rightarrow nX ( + m SM ) , \quad (3.11)$$

where  $n, m \in \mathbb{Z}^+$  count the multiplicity of  $X$  and SM particles, respectively, in the final states. The first decay channel is desired for dumping entropy into the visible sector and dilutes the primordial thermal population of  $X$ . If this were the only final state of  $Y$  decay, the resulting  $X$  would remain a purely thermal distribution with a temperature  $T_X$ , which would be relatively lower than the counterpart in the absence of dilution.

The other decay mode, whose branching ratio is assumed to be  $\text{Br}_X$ , produces a secondary non-thermal population of  $X$  that also contributes to the final dark matter relic abundance. The bracket in (3.11) also includes the possibility that this second decay channel is completely dark, without any ‘‘SM’’ in the final state. In the absence of extended dark sectors, the branching ratio of the first channel is simply  $1 - \text{Br}_X$ . With a nonzero  $\text{Br}_X$ , the final dark matter relic density becomes

$$\Omega_X \simeq 0.26 (1 + n\text{Br}_X) \left( \frac{m_X}{1 \text{ keV}} \right) \left( \frac{2.2 \text{ GeV}}{m_Y} \right) \sqrt{\frac{1 \text{ sec}}{\tau_Y}} . \quad (3.12)$$

Requiring  $\Omega_X$  to agree with the *Planck* measured value fixes  $\tau_Y$  in terms of  $m_X$  and  $m_Y$ , we can rewrite Eq. (3.7) as

$$T_{\text{RH}} \simeq \frac{0.4 \text{ MeV}}{g_*(T_{\text{RH}})^{1/4}} \frac{m_Y}{10^6 m_X} . \quad (3.13)$$

Because  $g_*$  is always larger than 1, and for successful big-bang nucleosynthesis to work, for which  $T_{\text{RH}} \gtrsim 1 \text{ MeV}$  is needed, the dilutor  $Y$  must be heavier than dark matter  $X$  by a factor of at least a million.

Before deriving and solving the equation for dark matter phase space distribution, we first give a qualitative discussion and introduce an important temperature relevant for large scale structure of the universe. Immediately after the  $Y \rightarrow nX + m SM$  decay, each secondary  $X$  particle roughly carries the energy of  $m_Y/(m+n)$ . Under the sudden decay approximation, the corresponding temperature of the universe is given by  $T_{\text{RH}}$  in Eq. (3.7). The velocity of  $X$  particles will then redshift with the expansion of the universe. After a while the  $X$  particles start to turn non-relativistic when the energy drops to around their mass. This requires the scale factor of the universe to grow by a factor of

$$\frac{a_{\text{NR}}}{a_{\text{RH}}} \simeq \frac{m_Y}{(m+n) m_X} . \quad (3.14)$$



The corresponding temperature  $T_{\text{NR}}$  can be found with entropy conservation in the SM sector

$$g_{*S}(T_{\text{NR}})T_{\text{NR}}^3 a_{\text{NR}}^3 = g_*(T_{\text{RH}})T_{\text{RH}}^3 a_{\text{RH}}^3, \quad (3.15)$$

which leads to

$$T_{\text{NR}} = T_{\text{RH}} \left( \frac{g_*(T_{\text{RH}})}{g_*(T_{\text{NR}})} \right)^{1/3} \frac{a_{\text{RH}}}{a_{\text{NR}}} \simeq 0.25 \text{ eV } n g_*(T_{\text{RH}})^{\frac{1}{12}}. \quad (3.16)$$

In the second step we used Eq. (3.13) and the late-time value for  $g_{*S}(T_{\text{NR}}) = 3.91$ , valid for  $T_{\text{NR}}$  well below the electron mass.

Note that  $T_{\text{NR}}$  defines the time when both the primordial  $X$  particles and the secondary ones from  $Y$  decay have become matter-like. Dialing the clock back to temperatures above  $T_{\text{NR}}$ , the dark matter fluid is made out of the non-relativistic primordial and the relativistic secondary component. The energy density of the latter is more important at temperatures above  $T_{\text{NR}}/\text{Br}_X$ . In this regime, the overall  $X$  fluid is relativistic and features a large pressure, which can interrupt the regular logarithmic growth of matter density perturbations in  $X$ . This suppresses the matter power spectrum  $P(k)$  for wavelengths of the perturbation smaller than the Hubble radius at temperature equal to  $T_{\text{NR}}/\text{Br}_X$ . The resulting  $P(k)$  may then potentially disagree with the LSS measurements, unless  $\text{Br}_X \ll 1$ .

#### D. Phase space distribution of dark matter

Let us go beyond the sudden decay approximation and derive the equations governing the dark matter phase space distribution. Because the temperature  $T_{\text{NR}}$ , when the secondary dark matter particles from dilutor decay turn non-relativistic, is found to be rather low, they act as a hot dark matter component for a period of time that overlaps with the observational data. Consequently, they may suppress the large and small scale structures, which in turn allows one to derive a powerful constraint on the dilutor  $\rightarrow$  dark matter branching ratio using cosmological data from the Sloan Digital Sky Survey (SDSS) [37].

Without loss of generality, we write the dilutor to dark matter decay channel as

$$Y \rightarrow X + 2 + 3 + \dots + N = n X + m \text{ SM}, \quad (3.17)$$

where particles  $2, 3, \dots, N = m + n$  represent either the SM or additional  $X$  particles in the final state. As before, we assume that  $nX$  particles are produced in this decay. The phase

space distribution for the produced  $X$  is governed by the Liouville's equation that relates the phase space distribution functions of dark matter  $f_X$  and the dilutor  $f_Y$

$$\left( \frac{\partial}{\partial t} - H \frac{|\vec{p}_X|^2}{E_X} \frac{\partial}{\partial E_X} \right) f_X(E_X, t) = \int \frac{d^3 \vec{p}_Y}{(2\pi)^3} \frac{1}{2E_Y} f_Y(E_Y, t) A, \quad (3.18)$$

$$A = \frac{1}{2E_X} \prod_{i=1}^N \int \frac{d^3 \vec{p}_i}{(2\pi)^3} \frac{1}{2E_i} (2\pi)^4 \delta^4 \left( p_Y - p_X - \sum_i p_i \right) |\mathcal{M}|^2. \quad (3.19)$$

Hereafter we work in the ultra-relativistic  $X$  limit (from  $Y$  decay) and approximate  $|\vec{p}_X| \simeq E_X$ .  $\mathcal{M}$  is the decay matrix element related to the decay in (3.17) and  $A$  can be rewritten in terms of the partial decay rate of  $Y \rightarrow X + \dots + N$  in its rest frame as

$$\Gamma_{Y \rightarrow X} = \frac{1}{2m_Y} \int \frac{d^3 \vec{p}_X}{(2\pi)^3} A = \frac{1}{4\pi^2 m_Y} \int dE_X E_X^2 A, \quad (3.20)$$

where it is assumed that the  $X$  particles from  $Y$  decay are ultra-relativistic throughout most of the phase space. Here it is useful to introduce a dimensionless spectral function  $g(\omega)$ , which satisfies

$$n \frac{d\Gamma_{Y \rightarrow X}}{d\omega} = \Gamma_{Y \rightarrow X} g(\omega), \quad \int d\omega g(\omega) = n, \quad \omega = \frac{E_X}{m_Y}. \quad (3.21)$$

It allows us to establish a relation between  $A$  and  $g$  and simplify the Liouville's equation to

$$\left( \frac{\partial}{\partial t} - H E_X \frac{\partial}{\partial E_X} \right) f_X(E_X, t) = \frac{4\pi^2}{E_X^2} \Gamma_{Y \rightarrow X} g\left(\frac{E_X}{m_Y}\right) \int \frac{d^3 \vec{p}_Y}{(2\pi)^3} \frac{1}{2E_Y} f_Y(E_Y, t). \quad (3.22)$$

Next, we assume that  $Y$  had already turned non-relativistic when the decay occurs, i.e.,  $E_Y \simeq m_Y$ . This is a necessary condition for the dilution mechanism to work, because  $Y$  is assumed to dominate the energy content in the universe as a matter component. It allows us to complete the  $p_Y$  integral in (3.22) and express it with the number density,  $n_Y(t) = \rho_Y(t)/m_Y$ .  $\rho_Y$  is the energy density of non-relativistic  $Y$  particles.

For the left-hand side of Eq. (3.22), we change the variables of  $f_X$  to  $x \equiv E_X/T_X$  and  $t$ , where  $T_X$  is the temperature of primordial  $X$  warm dark matter defined above. The appealing reason for such a change is that as long as the  $X$  particles remain ultra-relativistic, the ratio  $E_X/T_X$  stays invariant in the expanding universe. Using the identity,

$$\left( \frac{\partial}{\partial t} - H E_X \frac{\partial}{\partial E_X} \right) f_X(E_X, t) = \frac{\partial}{\partial t} f_X(x, t), \quad (3.23)$$

we finally obtain the phase space equation for secondary dark matter from dilutor decay,

$$\frac{T_X^3}{2\pi^2} x^2 \frac{\partial}{\partial t} f_X(x, t) = n_Y(t) \Gamma_{Y \rightarrow X} \frac{T_X}{m_Y} g\left(\frac{T_X}{m_Y} x\right). \quad (3.24)$$

This equation is to be solved along with the following set of energy density Boltzmann equations for  $X$ ,  $Y$  and the SM particles

$$\dot{\rho}_Y + 3H\rho_Y = -\Gamma_Y\rho_Y, \quad (3.25)$$

$$\dot{\rho}_X + 4H\rho_X = y\text{Br}_X\Gamma_Y\rho_Y, \quad (3.26)$$

$$\dot{\rho}_{\text{SM}} + \left(4H - \frac{\dot{g}_*}{3g_*}\right)\rho_{\text{SM}} = (1 - y\text{Br}_X)\Gamma_Y\rho_Y, \quad (3.27)$$

where  $\rho_{\text{SM}}$  is the energy density carried by relativistic visible particles and  $H^2 = 8\pi G_N(\rho_Y + \rho_X + \rho_{\text{SM}})/3$  is the Hubble parameter. This set of equations applies for non-relativistic  $Y$ , while the  $X$  population remains ultra-relativistic.

Using  $T_X$  to keep track of time, the phase space function  $f_X$  at late times can be solved

$$f_X(x) = \frac{1}{e^x + 1} + \frac{2\pi^2}{x^2} \frac{\Gamma_Y\text{Br}_X}{m_Y^2} \int_{T_{\text{fin}}}^{T_{\text{ini}}} \frac{dT_X}{T_X} \frac{\rho_Y}{T_X^2 H} g\left(\frac{T_X}{m_Y}x\right). \quad (3.28)$$

The first term of (3.28) is the primordial Fermi-Dirac distribution of  $X$  and the second is the non-thermal re-population of  $X$ . The  $T_X$  integral should cover the entire temperature range relevant for the production of the secondary component of dark matter. It goes from an arbitrary high initial temperature  $T_{\text{ini}}$ , which in practice we take  $T_{\text{ini}} = m_Y/10$  in order for  $Y$  to already be non-relativistic, as assumed below (3.22). The final result is insensitive to the exact choice of  $T_{\text{ini}}$ , because the  $\rho_Y/(T_X^2 H)$  factor in the integrand is suppressed at higher  $T_X$ , as long as  $T_X \ll m_Y$ . Moreover, the  $g$  function cannot lift this suppression, because  $T_X$  is bounded from above for a given fixed  $x$ .

On the lower limit of integration, we need to go to sufficiently low temperatures, such that all of the  $Y$  is depleted by decays into SM and  $X$ . Because of the exponential suppression in  $\rho_Y$ , the exact  $T_{\text{fin}}$  is also not relevant. In practice we integrate down to temperatures corresponding to  $t = 10\tau_Y$ , which sufficiently covers the entire period of non-relativistic  $Y$  decay.

The resulting distributions  $f_X$  are shown in FIG. 2, which are plotted at late times after the dilution has completed. The two options for two and three body decays correspond to two scenarios that are relevant for the minimal LRSM under consideration in this work.

1. The case when  $X$  is the lightest right-handed neutrino  $N_1$  and  $Y$  is a heavier  $N_2$ , which undergoes a three-body decay into  $N_1$  plus two charged leptons, mediated by the  $W_R$  gauge boson;

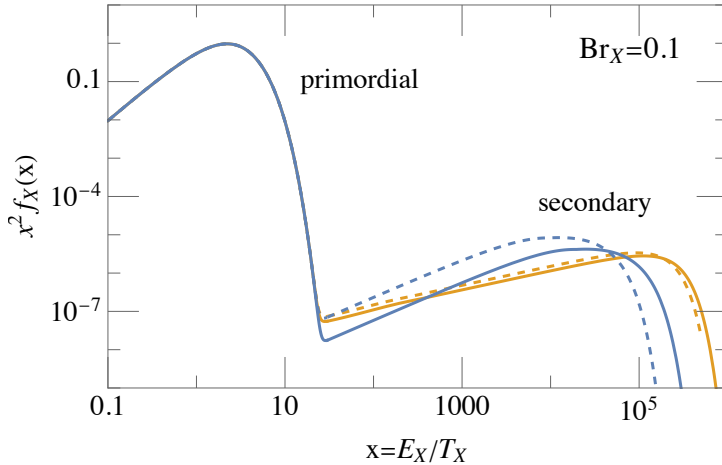


FIG. 2. Phase space distribution of ultra-relativistic dark matter species  $X$ . The blue (orange) curve corresponds to the three-body (two-body) decay model listed in TAB. I. Solid (dashed) curve corresponds to  $m_X = 10$  keV,  $m_Y = 100$  GeV ( $m_Y = 1$  PeV), while  $\text{Br}_X = 0.1$  for all the cases.

2.  $Y$  is a long-lived scalar  $\Delta_R$  with a partial decay width into two  $N_1$ .

The corresponding  $g$  functions and  $n, y$  integrals are summarized in TAB. I, where the masses of final-state charged leptons were neglected.

It is clear from FIG. 2 that the primary component of dark matter dominates at small  $x$ , while the secondary component features a significantly smaller occupancy, but carries more energy and thereby affects structure formation. On the plotted curves we kept fixed  $m_X$  and  $\text{Br}_X$  and took two different values of  $m_Y$  to demonstrate that the shape of the secondary component is roughly independent of the mass of the dilutor. This follows from Eqs. (3.12), where the relic density requires the scaling  $m_Y \sim 1/\sqrt{\tau_Y}$  and the reheating temperature is set by the Hubble time  $T_{\text{RH}} \sim \sqrt{H} \sim 1/\sqrt{\tau_Y}$ . Immediately after  $Y \rightarrow X$  decay,  $E_X \lesssim m_Y$  and  $T_X \sim T_{\text{RH}}$ . As a result, the kinematic endpoint  $x_{\text{max}} \sim m_Y/T_{\text{RH}}$  is roughly held constant for fixed  $m_X$ , irrespective of the values of  $m_Y$  or  $\tau_Y$ .

In the case where the dilutor is a long-lived scalar  $\Delta$  (see sec. IIB5), the kinematics is so simple that we can further derive an explicit closed form for  $f_X$ . Since it is a two body

dark matter $X$	dilutor $Y$	$Y \rightarrow X$ decay	$n$	$g(\omega)$	$y$
$N_1$	$N_2$	$N_2 \rightarrow N_1 + SM$	1	$16\omega^2(3 - 4\omega)\theta(\frac{1}{2} - \omega)$	$\frac{7}{20}$
$N_1$	$\Delta$	$\Delta \rightarrow N_1 N_1$	2	$2\delta(\omega - 1/2)$	1

TABLE I. The energy fraction distribution  $g(\omega)$ , taken away by dark matter  $X$  in the rest frame of the decaying dilutor  $Y$ , and its integrals  $n = \int g, y = \int \omega g$ . In the context of LRSM, the first row corresponds to  $N_2$  as dilutor which can undergo a three-body decay into a  $N_1$  plus two charged leptons ( $n = 1$ ) and  $\theta$  is the Heaviside unit step function. The second corresponds to the Majorana scalar boson  $\Delta$  dilution scenario, where each  $\Delta \rightarrow N_1 N_1$  produces two dark matter states ( $n = 2$ ) and  $\delta$  is the Dirac delta function.

decay,  $g$  is a Dirac- $\delta$  function and we can complete the  $T_X$  integral in Eq. (3.28) to obtain

$$x^2 f_X(x) = \frac{x^2}{e^x + 1} + \frac{8\pi^2 \text{Br}_X \Gamma_Y}{m_Y^2} \left( \frac{\rho_Y}{T_X^2 H} \right)_{T_{X^*}}, \quad (3.29)$$

$$\simeq \frac{x^2}{e^x + 1} + 0.16 \text{ sec Br}_X \left( \frac{10 \text{ keV}}{m_X} \right)^2 \left( \frac{\rho_Y}{T_X^2 H} \right)_{T_{X^*}}, \quad (3.30)$$

where we used the relic equation (3.12), set  $\Omega_X = 0.26$  and approximated with small  $\text{Br}_X$  in the second step. With such a simple expression in (3.30) we can understand the behaviour of  $f_X$  in FIG. 2 that emerges from solving Eq. (3.28). First of all,  $g$  is a  $\delta$  function in temperature, which essentially selects a particular moment in  $T_{X^*} = m_Y/(2x)$  for a fixed  $x$  and thus completely removes any dependence on the boundary conditions  $T_{\text{ini, fin}}$ .

Furthermore, we can derive the explicit dependence on  $x$  for various moments in the expansion of the universe during the dilutors' decay. For this, we only have to examine the  $x$  dependence of the factor  $(\rho_Y/T_X^2 H)_{T_{X^*}}$  in Eq. (3.30); the re-scaling with  $\Omega_X$  and  $m_X$  is trivial. Note that for the purpose of this discussion,  $Y$  is always non-relativistic and  $\rho_Y \propto m_Y T_X^3$ . In the early stages of radiation domination we have  $H \propto T_X^4$  and therefore  $(\rho_Y/T_X^2 H)_{T_{X^*}} \propto m_Y/T_{X^*} \sim x$ . Once  $Y$  starts to dominate, the Hubble parameter goes as  $H \sim \sqrt{\rho_Y}$  and the relevant term goes as  $(\rho_Y/T_X^2 H)_{T_{X^*}} \propto \sqrt{m_Y/T_{X^*}} \sim \sqrt{x}$ . In both cases,  $m_Y$  cancels out, that is why the orange curve in FIG. 2 remains almost identical for different choices of  $m_Y$ . Finally, large  $x$  corresponds to low  $T_{X^*}$  when all the  $Y$  has decayed away and the secondary part of  $f_X$  is exponentially suppressed. These  $x$  dependencies explain the shape of the 2-body orange curves in the  $x > 10$  region.

For the three-body decay, the spectral function  $g$  is not as sharply peaked as the Dirac  $\delta$ , but has a maximum at  $\omega = 1/2$  and similar considerations go through, with transitions between different  $x$  dependencies becoming less sharp. The bottom-line is that, once we fix  $Br_X$  and  $m_X$ , the  $f_X$  does not depend on the mass of the dilutor  $Y$ , the behavior of  $f_X$  is roughly the same for different decay topologies and it extends to large  $x$ , beyond the usual primary component. In the following section we will examine how this behaviour translates onto the physical matter power spectrum  $P(k)$ .

Let us emphasize that we assume the  $X$  particles remain collisionless after the  $Y$  decay throughout this work. This means that the imprint of the dark matter model (fundamental physics) on the phase space distribution is preserved until later times and can directly affect cosmological observations. We do not consider the possibility of having strong DM self-interactions. They could re-thermalize the dark sector and soften the above phase space distribution. At the same time, they would facilitate excessive dark matter production, which is adverse to the dilution mechanism considered here.

### E. Imprint on the matter power spectrum

Let us turn to a quantitative numerical analysis in the parameter space of  $m_X$  versus  $m_Y$ . For each point we first set the dilutor lifetime  $\tau_Y$  using Eq. (3.13). Next, we determine the phase space distribution  $f_X$  with Eq. (3.28) and evolve the density perturbations using the linear Boltzmann solver code CLASS [84–86] to obtain the corresponding matter power spectrum  $P(k)$ . We scan over 200 points in the mass range  $m_X \in (1 \text{ keV}, 1 \text{ MeV})$  and  $m_Y \in (1 \text{ GeV}, 10^{16} \text{ GeV})$  for both decay channels considered in TAB. I. The results are shown by the colored curves in FIG. 3, where we set  $Br_X = 0.1$ . The black solid curve is the fiducial  $\Lambda$ CDM model.

The experimental data points come from the SDSS DR7 on luminous red galaxies [87] (blue) and the Lyman- $\alpha$  forest [88] (orange) measurements. All the curves in scenarios with secondary  $X$  share a common feature with significant deviations from data in the  $k \gtrsim 0.03 h/\text{Mpc}$  region. These occur at a much lower  $k$  compared to other dark matter production mechanisms such as thermal freeze-in [89, 90]. This is mainly due to the large hierarchy between the dilutor and the dark matter mass, required by Eqs. (3.13). Based on a simple  $\Delta\chi^2$  fit to the data, we find that the LSS data from SDSS sets a much stronger

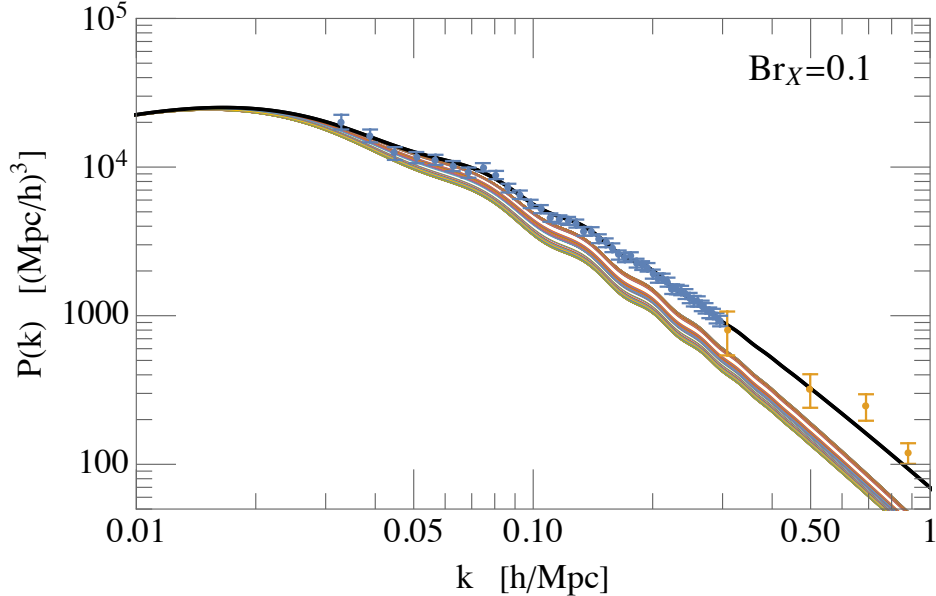


FIG. 3. Primordial matter power spectrum in standard  $\Lambda$ CDM (black solid curve) and a set of diluted dark matter models listed in TAB. I (colorful curves). Like in FIG. 2, we set  $\text{Br}_X = 0.1$ . Data points from SDSS DR7 LRG and Lyman- $\alpha$  observations are shown in blue and orange, respectively.

constraint on these scenarios than Lyman- $\alpha$ , making this probe particularly robust. The conflict with data increases with  $\text{Br}_X$ , which translates into an upper bound, shown in FIG. 4 for the two models in TAB. I. The bound does not depend much on the precise shape of the phase space distribution (because it is integrated over) and the message is similar for both cases: the branching ratio of the dilutor decaying into dark matter is constrained to be

$$\text{Br}_X \lesssim 1\%, \quad @95\% \text{ CL}. \quad (3.31)$$

This bound is nearly independent of  $m_Y$ , simply because the secondary component of the phase space distribution  $f_X$  in (3.28) is mostly independent of  $m_Y$ , as explained in the paragraph below (3.28). The  $\text{Br}_X$  limit gets slightly relaxed for larger  $m_Y$ , because holding the dark matter relic density fixed in Eq. (3.13) requires the lifetime  $\tau_Y$  to be shorter, leading to a higher reheating temperature after the decay of dilutor. The corresponding temperature for the secondary dark matter component to become non-relativistic also increases, which is a  $\sqrt[3]{g_*}$  effect, see Eq. (3.16). Eventually, this shifts the deviation of  $P(k)$  to a slightly higher  $k$ , where the data is less precise and thus becomes less constraining.

The constraint derived here comes predominantly from the LSS data, which relies only

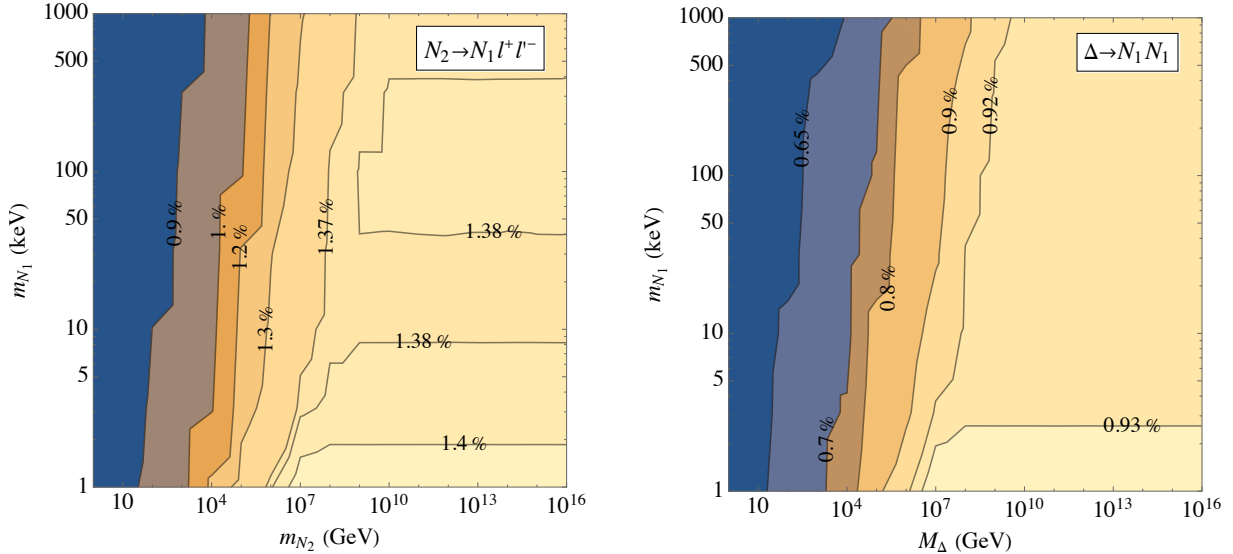


FIG. 4. Upper bound on  $\text{Br}_X$ , the branching ratio of dilutor  $Y$  decaying into  $X$  from the fit to LSS data (SDSS DR7 LRG), for the two dilution scenarios considered in TAB. I in the context of LRSM. For each point in the  $m_X - m_Y$  parameter space, the  $Y$  lifetime is determined by requiring  $X$  to comprise all of the dark matter in the universe.

on the evolution of matter density perturbations in the linear regime. LSS thus provides a robust test of these models and we expect similar constraints to apply broadly for other dilutor  $\rightarrow$  dark matter decay topologies.

Our result can be generalized to initial abundances for  $Y$  and  $X$  beyond the relativistic freeze-out. A sub-thermal initial population of  $Y$  needs to be heavier and/or longer lived in order to provide the same amount of entropy injection. The secondary  $X$  particles from  $Y$  decay become more energetic and take even longer to become matter-like. This impacts the primordial matter power spectrum down to even lower  $k$  and leads to a more stringent constraint on  $\text{Br}_X$  than Eq. (3.31). On the contrary, starting with a smaller overpopulation of  $X$ , the constraint on  $\text{Br}_X$  will be weaker.

#### IV. ANATOMY OF DILUTION SCENARIOS IN LRSM

Remarkably, the minimal LRSM contains all the ingredients for the dark matter dilution mechanism, described in the previous section, to occur. Throughout this work, we consider



the lightest right-handed neutrino  $N_1$  to be the dark matter, i.e.,

$$X = N_1. \quad (4.1)$$

Following the discussion in section II B 2, with a mass below 100 MeV, it always freezes out relativistically and is generically overproduced. The role of the diluting particle  $Y$  can be played by either a heavier right-handed neutrino or the Majorana Higgs boson  $\Delta$ ; the latter option is explored here for the first time. In this section, we carefully examine the viability of each scenario and point out the corresponding opportunities for experimental tests.

### A. Heavy neutrino dilutor

In this subsection, we first consider one of the two heavier right-handed neutrinos  $N_2$  to play the role of the dilutor  $Y$ . We begin with the implications of LSS constraint obtained from the previous section, which results in a non-trivial no-go theorem. We then discuss the options for bypassing such constraints and describe the viable scenarios.

#### 1. Implication of the SDSS constraint

Let us label the dilutor of section IV A as  $Y = N_2$ . The most obvious decay channels of  $N_2$  are those mediated by the heavy  $W_R$  boson in the LRSM. Corresponding Feynman diagrams for the decays are depicted in FIG. 5 below. Similarly to weak decays of the  $\tau$  lepton in the SM, there are semi-leptonic and pure-leptonic decay channels.

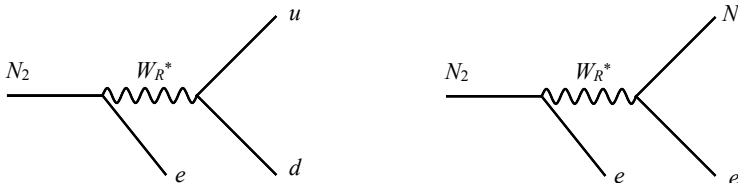


FIG. 5. Feynman diagram for dilutor  $N_2$  decay via right-handed charged-current interaction mediated by  $W_R$ . The flavor or final state charged leptons and quarks is dictated by the matrix elements of  $V_{\text{PMNS}}^R$  and  $V_{\text{CKM}}^R$ .

All the decay products in the first channel are SM particles, which makes it a perfect decay mode for the DM dilution mechanism to work. In contrast, the second channel has

a dark matter  $N_1$  in the final state. The corresponding decay branching ratio is tightly constrained by large scale structure observations, to be smaller than 1%, as pointed out in section III E.

In the minimal LRSM, the ratios among the above  $W_R$  mediated decay are fixed by the structure (particle content and gauge interactions) of the model. If these were the only  $N_2$  decay channels, the decay branching into the final state containing  $N_1$  would be 10% for mass of  $N_2$  well above the electroweak scale. This branching ratio only gets higher for lighter  $N_2$ . The large scale structure constraint from SDSS thus firmly excludes such simplest dilution scenario. What may save the day are other possible decay channels of  $N_2$ . These may arise either due to neutrino or gauge boson mixing in the LRSM, as will be discussed next.

## 2. A no-go theorem

If minimality is one's first priority, it would be most desirable to open up the extra decay channel(s) for the right-handed neutrino dilutor and also allow it to participate in the type-I seesaw mechanism for generating the active neutrino masses. Naïvely, both could occur through a mixing of  $N_2$  with the active neutrinos. However, there is a no-go theorem against such a possibility.

If the dilutor  $N_2$  participates in the seesaw mechanism, the mixing between  $N_2$  and light neutrinos is bounded from below

$$\theta_{N_2\nu} \gtrsim \sqrt{\frac{m_\nu}{m_{N_2}}}. \quad (4.2)$$

The value of  $\theta_{N_2\nu}$  could be much larger than  $\sqrt{m_\nu^\odot/m_{N_2}}$  due to additional degrees of freedom involved in type-I seesaw mechanism [91], but cannot be made smaller if  $N_2$  is responsible for neutrino mass generation. For this contribution to the neutrino mass to be significant and at least explain the mass difference for solar neutrino oscillation, we require  $m_\nu \gtrsim m_\nu^\odot \simeq \sqrt{8 \times 10^{-5} \text{ eV}^2}$ .

We first consider the case where the  $N_2$  mass lies below the weak scale. The partial decay width of  $N_2$  via this mixing and an off-shell  $W$  boson is then

$$\tau_{N_2}^{-1} \gtrsim \frac{\mathbf{m} G_F^2 m_{N_2}^5 \theta_{N_2\nu}^2}{96\pi^3} \gtrsim 10^{-23} \text{ GeV} \left( \frac{m_{N_2}}{1 \text{ GeV}} \right)^4, \quad (4.3)$$

where  $\mathbf{m}$  is the final state multiplicity factor within the range  $\sim 1 - 10$ . In the first step, we neglect contributions to the decay via the  $Z$  boson or possible interference effects. This

approximation would only affect our estimate by an order one factor, but keep our conclusion intact. The first inequality also accounts for other possible (subdominant)  $N_2$  decay channels (e.g., via  $W_R$ ) and the second inequality follows from Eq. (4.2). Plugging Eq. (4.3) into Eq. (3.12), we find a lower bound on the dark matter relic density

$$\Omega_{N_1} \gtrsim 2.9 \left( \frac{m_{N_1}}{6.5 \text{ keV}} \right) \left( \frac{m_{N_2}}{1 \text{ GeV}} \right). \quad (4.4)$$

The reference mass for  $N_1$  is the lower bound on warm dark matter found by the DES collaboration [3], which is consistent with other constraints using the Lyman- $\alpha$  forest [29, 30], strong gravitational lensing observations [31, 32], and recent combined analysis [33, 34]. The observed dark matter relic abundance then sets an upper bound on the mass of  $N_2$ ,

$$m_{N_2} \lesssim 90 \text{ MeV}. \quad (4.5)$$

Applying this bound again back in Eq. (3.12), we obtain a lower bound on the lifetime of  $N_2$ ,

$$\tau_{N_2} \gtrsim 160 \text{ sec}. \quad (4.6)$$

Because the universe was matter-dominated before the  $N_2$  decayed away, the above lower bound on its lifetime is strongly excluded by the big-bang nucleosynthesis, which would require  $\tau_{N_2} \lesssim 1 \text{ sec}$ .

On the other hand, if  $N_2$  is heavier than the weak scale, the decay induced by the mixing parameter Eq. (4.2) would be into an on-shell  $W$  boson at a much higher rate,

$$\tau_{N_2}^{-1} \gtrsim \frac{G_F m_{N_2}^3 \theta_{N_2\nu}^2}{4\sqrt{2}\pi} \left( 1 - \frac{M_W^2}{m_{N_2}^2} \right) \left( 1 + \frac{M_W^2}{m_{N_2}^2} - \frac{2M_W^4}{m_{N_2}^4} \right) \gtrsim 10^{-12} \text{ GeV} \left( \frac{m_{N_2}}{100 \text{ GeV}} \right)^2. \quad (4.7)$$

The factor  $G_F m_{N_2}^2$  properly accounts for a longitudinal enhancement in the limit when  $m_{N_2} \gg M_W$ . Plugging this into Eq. (3.12) leads to a lower bound on the dark matter relic density

$$\Omega_{N_1} \gtrsim 1.7 \times 10^5 \left( \frac{m_{N_1}}{6.5 \text{ keV}} \right). \quad (4.8)$$

All the  $N_2$  mass dependency cancels out completely and dark matter is considerably over-produced.

This completes the proof of the no-go theorem. It is derived by combining the constraints on the dark matter relic density and the dilutor lifetime. Although we have used some  $\sim$  in the above reasoning, the results in Eqs. (4.6) and (4.8) are in sharp contradiction with the

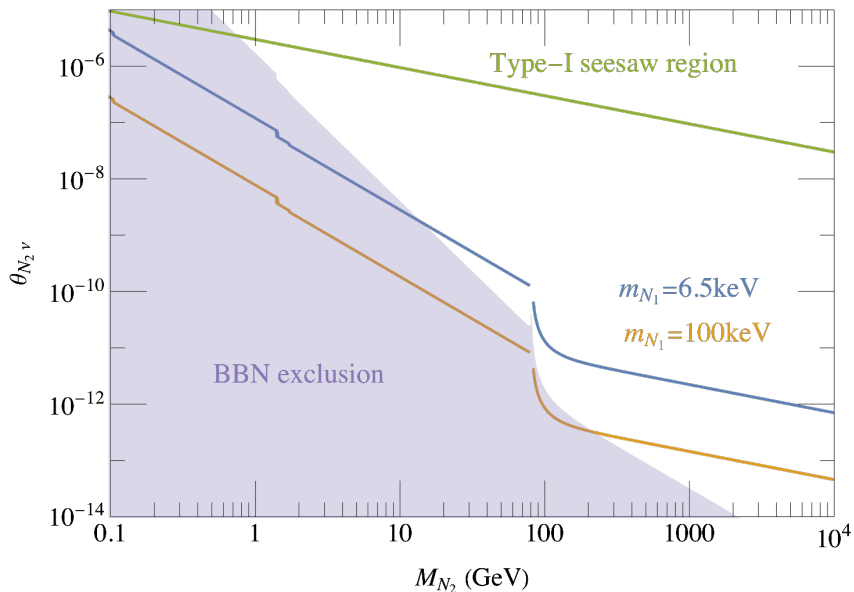


FIG. 6. Parameter space for correct dark matter relic density, where  $N_2$  serves as the dilutor and decays via a mixing with the active neutrino. We obtain  $\Omega_{N_1} = 0.26$  along the blue and orange curves for  $m_{N_1} = 6.5$  and 100 keV, respectively. The purple shaded region is excluded by BBN, because the lifetime of  $N_2$  is longer than a second. Along with the relic curves, it sets an upper bound on the mixing  $\theta_{N_2\nu}$ . This upper bound is stronger for heavier  $N_1$ . In contrast, the region above the green line in the upper-right corner of the figure shows the mixing angle needed for  $N_2$  to participate in the type-I seesaw mechanism and explain the neutrino mass difference for solar neutrino oscillation. This is clearly incompatible with the dilution mechanism and verifies the no-go theorem presented in section IV A 2.

existing constraints, making it convincing there is no room to avoid the theorem. It is also worth pointing out that the theorem not only applies to the LRSM focused in this work, but also to other gauge extensions, such as the  $U(1)_{B-L}$  model [26, 92, 93].

### 3. Type-II seesaw dominance and dilutor decay via $N - \nu$ mixing

The no-go theorem presented above implies that if one of the heavier right-handed neutrinos (e.g.,  $N_2$ ) plays the role of dilutor, its mixing with light active neutrinos must be much smaller than Eq. (4.2). In other words, the contribution to neutrino mass from  $N_2$

via the type-I seesaw must be well below what is needed for explaining the observed neutrino oscillation phenomena. At the same time, the dark matter candidate  $N_1$  also cannot fully participate in the seesaw, because of the X-ray constraints. The only remaining right-handed neutrino  $N_3$  is free from constraints and does contribute to neutrino masses in the type-I seesaw, but is unable to explain the two mass square differences needed for neutrino oscillations. As a consequence, light neutrino masses must be accounted for by additional sources <sup>4</sup>.

A way out within the minimal LRSM is by considering another source of mass for the light neutrinos, which comes from the vacuum condensate of the left-handed scalar triplet  $\Delta_L$ , through the type-II seesaw mechanism. By relieving the dilutor  $N_2$  from the role of neutrino mass generation, we can treat its mixing with light neutrinos  $\theta_{N_2\nu}$  as a free parameter, which can be arbitrarily small. This enables a viable window in the model parameter space for the dark matter dilution mechanism to work.

In FIG 6, the blue and orange curves show where in the  $\theta_{N_2\nu}$  versus  $m_{N_2}$  plane the dark matter  $N_1$  can obtain the correct relic density after the  $N_2$  dilution, for two choices of  $N_1$  mass. The value 6.5 keV is the lowest allowed warm dark matter mass by the DES result. The purple region is excluded by BBN because the lifetime of  $N_2$  is longer than a second. Clearly, viable values of  $\theta_{N_2\nu}$  must be very tiny  $\lesssim 10^{-9}$  to satisfy both constraints. In contrast, the region above the green line indicates the required values of  $\theta_{N_2\nu}$  if  $N_2$  participates in the type-I seesaw mechanism, which offers a way to visualize and quantify the above no-go theorem. We also find a lower bound on the dilutor  $N_2$  mass of around 20 GeV.

The dark matter relic curves in FIG. 6 are valid under the assumption that the  $W_R$  mediated decay modes of the dilutor  $N_2$  (see FIG. 5) are subdominant to those induced by the  $N_2 - \nu$  mixing. This condition is mostly easily satisfied if  $N_2$  is heavier than the  $W$  boson but still close to the weak scale. This leads to a lower bound on the mass scale of  $W_R$  boson,

$$M_{W_R} \gtrsim \frac{10 \text{ GeV}}{\sqrt{\theta_{N_2\nu}}} \gtrsim 10^6 \text{ GeV} = 1 \text{ PeV} , \quad (4.9)$$

where in the second step we read from FIG. 6 that for  $m_{N_2} > M_W$ , the highest value of  $\theta_{N_2\nu}$  is around  $10^{-10}$ , which is also orders of magnitude below the seesaw line, required for

<sup>4</sup> This argument also implies that the minimal  $U(1)_{B-L}$  model where the new gauge symmetry is broken by a Standard Model singlet scalar is unable to account for both the dark matter dilution mechanism and neutrino masses. Additional degrees of freedom (e.g. the counterpart of  $\Delta_L$ , see below) are needed.

neutrino mass generation.

#### 4. Dilutor decay via $W - W_R$ mixing and X-ray limits

The previous subsections explored the possibility of the dilutor  $N_2$  decaying dominantly through its mixing with the active light neutrinos. Here, we discuss another possible  $N_2$  decaying channel inherent to the minimal LRSM, via the gauge boson mixing  $\xi_{LR}$ , mentioned in section II B 4 and shown in the Feynman diagram on FIG. 7 below. Because the absolute value of  $\xi_{LR}$  is bounded from above by  $M_W^2/M_{W_R}^2$  (see Eq. (2.11)), if  $N_2$  is lighter than the  $W$  boson and decays via off-shell  $W$ , the corresponding partial decay rate will have the same parametric dependence as those in Fig. 5. It cannot provide sufficient suppression to the branching ratio of  $N_2 \rightarrow N_1$  decay and the resulting dark matter production/dilution mechanism still suffers from the strong constraint from large scale structure. This observation forces the viable parameter space to the window where  $M_{W_R} > m_{N_2} > M_W$ .

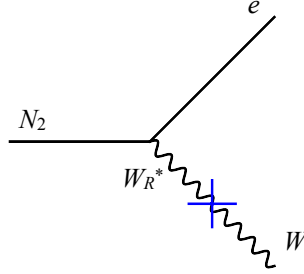


FIG. 7. Feynman diagram for  $N_2$  decay via  $W - W_R$  mixing in LRSM. Blue cross indicates an insertion of  $\xi_{LR}$  mixing.

In this case, the available decay rates for  $N_2$  are

$$\begin{aligned} \Gamma_{N_2 \rightarrow N_1 \ell^+ \ell'^-} &= \frac{G_F^2 m_{N_2}^5}{96\pi^3} \left( \frac{M_W}{M_{W_R}} \right)^4, & \Gamma_{N_2 \rightarrow \ell q \bar{q}'} &= \frac{\mathbf{m} G_F^2 m_{N_2}^5}{96\pi^3} \left( \frac{M_W}{M_{W_R}} \right)^4, \\ \Gamma_{N_2 \rightarrow \ell W} &= \frac{g^2 |\xi_{LR}|^2 m_{N_2}}{32\pi} \left( \frac{m_{N_2}}{M_W} \right)^2 \left( 1 - \frac{M_W^2}{m_{N_2}^2} \right) \left( 1 + \frac{M_W^2}{m_{N_2}^2} - \frac{2M_W^4}{m_{N_2}^4} \right), \end{aligned} \quad (4.10)$$

where the first two decays occur via diagrams in FIG. 5 and the last one via FIG. 7. Again,  $\mathbf{m}$  is the final state multiplicity factor, which equals 12 (9) for  $m_{N_2} > (<) m_t + m_b$ . In the absence of  $\theta_{N_2 \nu}$ , the three rates in (4.10) sum up to the total decay rate of  $N_2$ .

Like before, we impose three requirements on the dilution scenario here:

1. Dark matter  $N_1$  obtains the correct relic density;

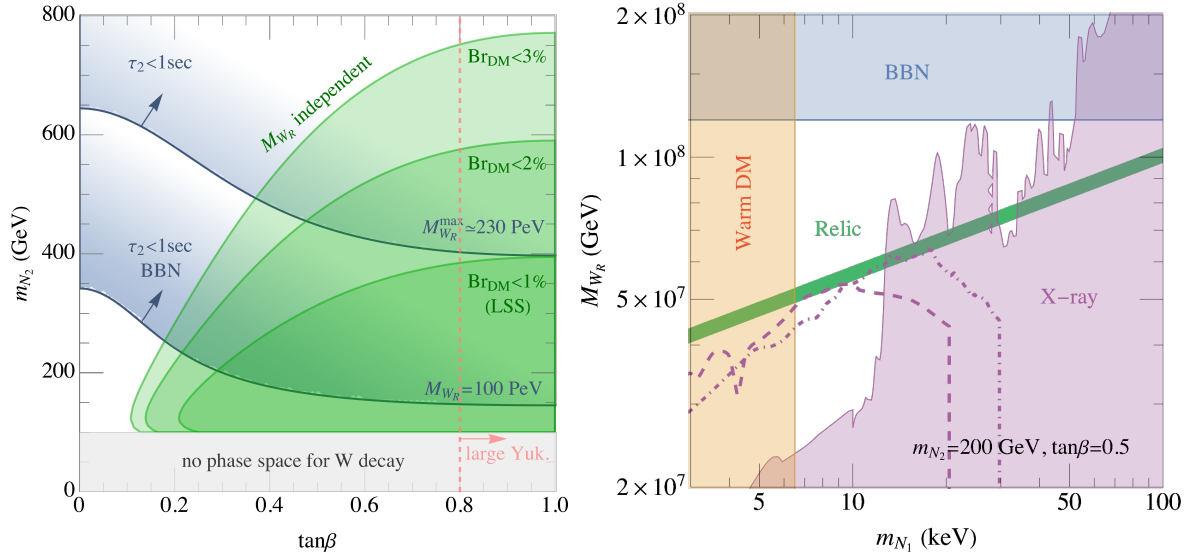


FIG. 8. Left: Viable parameter space for the dark matter dilution to work in the  $m_{N_2}$  versus  $\tan\beta$  plane, where the diluting particle  $N_2$  dominantly decays via the mixing between  $W$  and  $W_R$  gauge bosons. The region outside the darkest green is excluded by the LSS constraint in Eq. (3.31). The region to the right of the vertical pined dashed line is excluded by the theoretical constraint on the range of  $\tan\beta$ , Eq. (2.14). The two dark blue curves corresponds to lower bound on  $m_{N_2}$  to pass the BBN constraint, for two choices of  $W_R$  mass,  $10^8 \text{ GeV}$  and  $2.25 \times 10^8 \text{ GeV}$ , respectively. Right: Further constraints in the  $M_{W_R}$  versus  $m_{N_1}$  plane, with other parameters fixed,  $m_{N_2} = 200 \text{ GeV}$  and  $\tan\beta = 0.5$ . The blue shaded region again indicates the upper bound on  $M_{W_R}$  from the BBN constraint. The purple region is excluded by the existing  $X$ -ray line searches for dark matter decay  $N_1 \rightarrow \nu\gamma$  via the loop processes shown in Fig. 11. The dashed and dot-dahsed purple curves corresponds to the reach of future  $X$ -ray experiments ATHENA and XRISM, respectively. The orange shaded region is the warm dark matter exclusion limit set by the DES experiment. The green band is where dark matter obtains the correct relic density after the entropy dilution.

2. The decay branching ratio of dilutor  $N_2$  to dark matter is smaller than 1%;
3. Dilutor decays faster than 1 second.

Our main results are then summarized in FIG. 8.

The left-panel shows the parameter space of  $m_{N_2}$  versus  $\tan\beta$ . Outside the darkest green shaded region, the dilutor to dark matter decay branching ratio exceeds 1% and the

parameter space is excluded by the LSS data. From Eq. (4.10), it is useful to note that the branching ratio and the LSS constraint is independent of other parameters of the model such as  $M_{W_R}$  or  $m_{N_1}$ . In contrast, the total decay rate of dilutor  $N_2$  does depends on  $M_{W_R}$  and so is the allowed parameter space that is consistent with the BBN constraint. The two blue curves show the lower limit on  $m_{N_2}$  for two choices of  $M_{W_R} = 10^8$  GeV (lower) and  $2.25 \times 10^8$  GeV (upper), respectively. Clearly, the latter case is marginal where the available parameter space for dilution mechanism closes. From this, we derive a upper bound on  $M_{W_R} < 2.25 \times 10^8$  GeV. In the same plot, the vertical pink dashed line corresponds to the theoretical upper bound on  $\tan\beta$  derived in Eq. (2.14). Viable parameter space for dark matter relic only occurs in the darkest green region with proper arrangement of other parameters.

Next, we address the  $X$ -ray line search limits on dark matter  $N_1$  decay, as shown on the right panel of FIG. 8. In the minimal LRSM, the dark matter candidate is not absolutely stable and there are in fact two contributions to the radiative decay of  $N_1 \rightarrow \nu\gamma$ . One is via the  $N_1$ - $\nu$  mixing and applies also to the regular sterile neutrino dark matter. The other is through the  $W - W_R$  mixing and both occur at the one loop level with coherent amplitudes. In the presence of a nonzero  $\theta_{N_1\nu}$ , the radiative decay rate of dark matter is a well known result [94, 95],

$$\Gamma_{N_1 \rightarrow \nu\gamma} = \frac{9\alpha\xi_{\text{LR}}^2}{256\pi^4} G_F^2 m_{N_1}^5 \sin^2 \theta_{N_1\nu}. \quad (4.11)$$

In the presence of a nonzero  $\xi_{\text{LR}}$ , there are new Feynman diagrams for the radiative decay of dark matter  $N_1$ . We derive the leading-order decay rate

$$\Gamma_{N_1 \rightarrow \nu\gamma} = \frac{\alpha\xi_{\text{LR}}^2}{8\pi^4} G_F^2 m_{N_1}^3 \sum_{\ell} |(V_{\text{PMNS}}^R)_{\ell 1}|^2 m_{\ell}^2. \quad (4.12)$$

See appendix A for a detailed derivation of this rate. In this case, because of the  $W_R$  and  $\tan\beta$  dependencies in  $\xi_{\text{LR}}$ , we find a closer interplay between the  $X$ -ray search bounds and the requirements on the dilution mechanism found in the previous subsection.

The implications from  $X$ -ray constraints are shown in FIG. 8 (right). We fix  $m_{N_2} = 200$  GeV and  $\tan\beta = 0.5$  which is an allowed point in FIG. 8 (left), and show the other constraint in the dark matter mass  $m_{N_1}$  versus  $M_{W_R}$  parameter space. As discussed earlier, for the dilutor  $N_2$  to decay before BBN, there is an upper bound on  $M_{W_R}$  for given  $m_{N_2}$ . This excludes the blue shaded region. The purple shaded region is then excluded by the existing  $X$ -ray line searches for dark matter decay [96–98], which sets a lower bound



on  $M_{W_R}$  and upper bound on  $m_{N_1}$ . Interestingly, the remaining window for viable dark matter in this scenario can be tested by the upcoming X-ray experiments ATHENA [99] and XRISM [100, 101], as shown by the dashed and dot-dashed purple curves. Here, we assume generic flavor mixing matrix where all the elements are  $\mathcal{O}(1)$  in magnitude and approximate  $\sum_\ell |(V_{\text{PMNS}}^R)_{\ell 1}|^2 m_\ell^2 \sim m_\tau^2$  in Eq. (4.12). The X-ray limit could be weakened if the right-handed leptonic mixing matrix element  $(V_{\text{PMNS}}^R)_{\tau 1}$  is suppressed or if destructive interference between amplitudes is strong enough. As explained in section III D (see also Eq. (3.28)), for sufficiently small  $\text{Br}_{Y \rightarrow X}$ , the phase space distribution of dark matter  $N_1$  follows exactly the thermal distribution, exactly like a warm dark matter is defined [102, 103]. The orange shaded region corresponds to a lower bound of 6.5 keV on warm dark matter mass.

#### 5. Lower bound on the $W_R$ mass scale

So far, we have discussed several options of having the light right-handed neutrino  $N_1$  to comprise all the dark matter in the universe, through the dilution mechanism where the dilutor is a heavier right-handed neutrino  $N_2$ . In all cases, we find that the mass scale of the  $W_R$  gauge boson must be rather high. In the case where  $N_2$  dominantly decays via its mixing with light neutrinos, the lower bound is around PeV scale, as found in Eq. (4.9). In the case where  $N_2$  dominantly decays via  $W - W_R$  gauge boson mixing, lower bound on  $M_{W_R}$  is higher (tens of PeV), due to the relic density explanation and constraints on the radiative decay of dark matter  $N_1$ , as shown in FIG. 8 (right). In both cases when calculating the decay rate of dilutor  $N_2$ , we have made the assumption that the masses of its decay products are much smaller than  $m_{N_2}$ . The lower bounds on  $M_{W_R}$  are derived based on this assumption, which are generic and does require special arrangement of the parameters of the model.

Here, we wish to scrutinize if the mass scale of  $W_R$  is allowed to be even lighter at all if some amount of tuning of parameters is arranged. While this might be less appealing, the main motivation behind is the prospect of other experimental probes (such as high-energy colliders) of the LR symmetry scale. Such a possibility was first explored in [36], which resorts to a compress spectrum with the mass of dilutor  $N_2$  being close to the sum of charged pion and a charged lepton masses. This leads to a phase space suppression in

the dilutor decay rate ( $N_2 \rightarrow \pi + \ell$ ) and enables sufficient longevity while keeping  $W_R$  mass near the TeV scale. Moreover, the flavor structure of the right-handed lepton mixing matrix  $V_{\text{PMNS}}^R$  must also be tuned, such that  $N_1$  primarily couples to the  $\tau$  lepton in the right-handed current interaction, thus kinematically forbidding the  $N_2 \rightarrow N_1$  decay (via off-shell  $W_R$ ) that is constrained by large scale structure as discussed in section IV A 1. In this scenario, light neutrino masses can be explained via a mixed type-I (where  $N_3$  mainly contributes) and type-II seesaw mechanism.

To explain the dark matter relic density using the dilution mechanism (see Eq. (3.12)), it seems challenging to have a dilutor  $N_2$  mass well below 2.2 GeV, because BBN forbids the lifetime of  $N_2$  to be longer than a second, while at the same time the Tremaine-Gunn bound forbids dark matter mass to be well below a keV. To get around this difficulty, [36] noticed a special mass window around  $M_{W_R} \sim 5$  TeV could work, where the above flavor structure allows dark matter  $N_1$  to freeze out slightly before the QCD phase transition whereas the dilutor  $N_2$  freezes out slightly after. It leads to an enhancement factor in the dilution factor  $\mathcal{S}$  in Eq. (3.9), given by the ratio of  $g_*$  at temperatures above and below  $\Lambda_{\text{QCD}}$ , and in turn a suppression in the final dark matter relic density. Thanks to this effect, [36] found viable solutions for dark matter mass around 0.5 keV. However, after the recent substantial progress in constraining the warm dark matter mass, e.g.  $m_{N_1} > 6.5$  keV, found by the DES collaboration from ultra-faint dwarfs [3], such a low mass  $W_R$  window has been firmly closed. This leads us to conclude that with a right-handed neutrino dilutor, the up-to-date lower bound on  $M_{W_R}$  for consistent dark matter cosmology in LRSM is pushed to above the PeV scale, given by Eq. (4.9).

## B. Majorana Higgs dilutor

In this subsection, we explore the other dilutor candidate in LRSM, the Majorana Higgs  $\Delta$ , introduced in section II B 5. The role of dark matter is still played by  $N_1$ . To our knowledge, such a possibility has not been considered in any previous dark matter analysis of the model.

Through the spontaneous gauge symmetry breaking  $SU(2)_R \times U(1)_{B-L} \rightarrow U(1)_Y$ , the couplings of  $\Delta$  are tied to mass generation of the gauge bosons  $W_R^\pm, Z'$  and the right-handed neutrinos  $N_i$ . To be long lived and qualify as the diluting particle, the mass of  $\Delta$  must be

well below those of  $W_R$  and  $Z'$ . We will work in the parameter space where  $\Delta$  is also much lighter than two of the right-handed neutrinos  $N_2, N_3$ . As a result, the decays of  $\Delta$  into these on-shell final state particles are forbidden. Its possible decay channels are shown by the Feynman diagrams in FIG. 9.

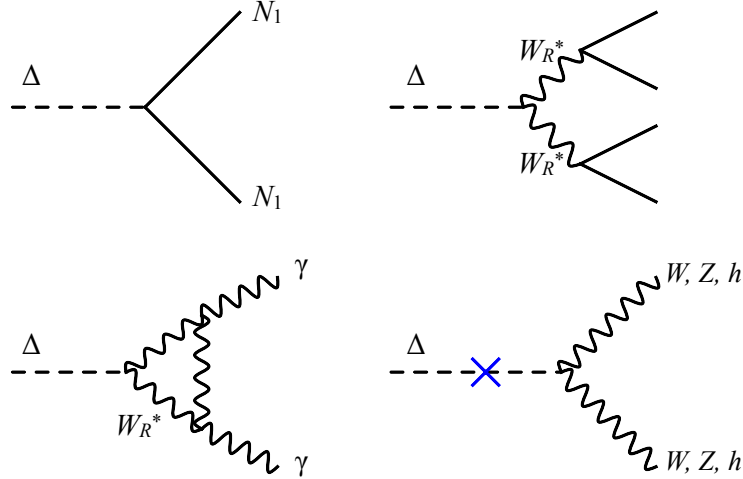


FIG. 9. Feynman diagrams for the decay rate of the dilutor  $\Delta$  in the minimal LRSM. The coupling of  $\Delta$  to right-handed neutrino and  $W_R^\pm$  are proportional to their masses, whereas the blue cross in the last diagram represents  $\Delta$ -Higgs boson mixing, generated by the scalar potential. In the second diagram, the fermion final states that connect to virtual  $W_R$  include quark pairs and  $N_1$  plus a charged lepton.

The decay rate of  $\Delta$  into two dark matter particles  $N_1$  is suppressed by the small mass  $m_{N_1}$ . The decays via off-shell  $W_R$  into light fermions or two photons are suppressed by the small ratio of  $M_\Delta/M_{W_R}$ . The decay via off-shell  $Z'$  is always subdominant, because  $Z'$  is heavier than  $W_R$  by a factor of  $\sqrt{3}$  and a relatively smaller decay branching ratio into  $N_1$  [104]. Finally,  $\Delta$  could decay via a mixing with the SM Higgs boson. For  $M_\Delta$  well above the electroweak scale, the dominant decays via the Higgs mixing are into  $W^+W^-$ ,  $ZZ$  and  $hh$  final states.

With the mass hierarchy  $M_W \ll M_\Delta \ll M_{W_R}$ , the partial decay rates of  $\Delta$  are

$$\begin{aligned} \Gamma_{\Delta \rightarrow N_1 N_1} &= \frac{G_F M_W^2 m_{N_1}^2 M_\Delta}{4\sqrt{2}\pi M_{W_R}^2}, & \Gamma_{\Delta \rightarrow W_R^* W_R^*} &= \frac{5G_F^3 M_W^6 M_\Delta^7}{576\sqrt{2}\pi^3 M_{W_R}^6}, \\ \Gamma_{\Delta \rightarrow \gamma\gamma} &= \frac{49\alpha^2 G_F M_W^2 M_\Delta^3}{128\sqrt{2}\pi^3 M_{W_R}^2}, & \Gamma_{\Delta \rightarrow h^*} &\simeq \frac{\theta_{\Delta h}^2 G_F M_\Delta^3}{4\sqrt{2}\pi}. \end{aligned} \quad (4.13)$$

For simplicity, we work in the limit where all final state particle masses are negligible. The  $\Delta \rightarrow W_R^* W_R^*$  decay occurs through two off-shell  $W_R^\pm$  bosons and has four right-handed fermions in the final states. For this partial rate, we apply the 4-body decay formula Eq. (2.35) of [105] and work in the heavy  $W_R$  limit. The kinematically allowed fermion final states are quark pairs and  $N_1$  plus a charged lepton.

Among the above four decay channels of the dilutor, the first two can produce energetic dark matter  $N_1$  in the final state and get constrained by the large scale structure observations. The third channel, where  $\Delta$  decays into a pair of photons, can bypass the LSS constraint. Indeed, we find that the ratios

$$\frac{\Gamma_{\Delta \rightarrow N_1 N_1}}{\Gamma_{\Delta \rightarrow \gamma \gamma}} \simeq 1.2 \times 10^{-7} \left( \frac{m_{N_1}}{M_\Delta} \right)^2, \quad \frac{\Gamma_{\Delta \rightarrow W_R^* W_R^*}}{\Gamma_{\Delta \rightarrow \gamma \gamma}} \simeq 2.3 \times \left( \frac{M_\Delta}{M_{W_R}} \right)^4, \quad (4.14)$$

can both be made much smaller than 1% if  $m_{N_1} \ll M_\Delta \ll M_{W_R}$ . This mass-scale hierarchy is consistent with the above mass spectrum assumptions. It allows the LRSM to evade the LSS constraint, even in the absence of  $\Delta$ -Higgs boson mixing.

In the left panel of FIG. 10, we first work in the  $\theta_{\Delta h} = 0$  limit and the blue and orange curves show the  $M_\Delta$  versus  $M_{W_R}$  parameter space, where dark matter  $N_1$  obtains the correct relic abundance through the  $\Delta$ -dilution mechanism, for two values of  $m_{N_1} = 6.5$  keV and 100 keV, respectively. We apply Eq. (3.10) by identifying  $Y = \Delta$ . Dark matter is overproduced in regions to the left of the curves. The purple region is excluded by LSS observations, because the branching ratio for  $\Delta \rightarrow W_R^* W_R^* \rightarrow$  light fermions decay is too high (see Eq. (4.14)). We find that the mass scale of  $W_R$  must be very high, above  $\sim 10^{11}$  GeV, but the mass scale of  $\Delta$  can be much lower. However, the price of having a lighter  $\Delta$  is to increase the mass hierarchy between  $\Delta$  and  $W_R$ , as indicated by the green dashed lines. Similar to the argument in footnote 2 against a very light  $\Delta$  to be the dark matter, we do not consider  $\Delta$  to be lighter than  $W_R$  by much more than a loop factor. Taking into account of this theoretical constraint, we end up finding that both  $\Delta$  and  $W_R$  masses are pushed to rather high values, close to the GUT scale. We have also checked that the lifetime of  $\Delta$  is much shorter than 1 second along the entire curves, thus safely evading the BBN constraint.

In the right panel of FIG. 10, we project the relic curves to the  $\theta_{\Delta h}$  versus  $M_\Delta$  parameter space for two realistic choices of the mass ratio  $M_{W_R}/M_\Delta$ . On each relic curve, the horizontal part has no  $\theta_{\Delta h}$  dependence because the total decay rate is dominated by  $\Delta \rightarrow \gamma\gamma$ . The decay via Higgs mixing takes over in the region with larger  $\theta_{\Delta h}$  and heavier  $\Delta$ . On each

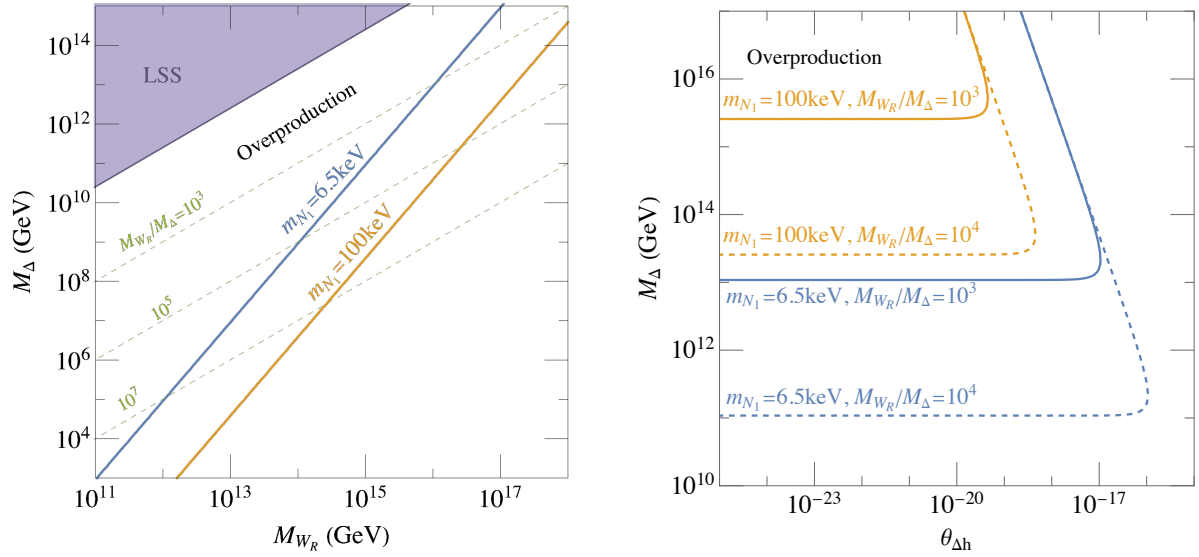


FIG. 10. Blue and orange curves show the parameter space where dark matter obtains the correct relic abundance via the dilution mechanism, where the Majorana Higgs  $\Delta$  plays the role of dilutor. In the left panel, we set  $\theta_{\Delta h} = 0$ . The purple region is excluded by the LSS observations. The green dashed curves indicate different  $M_{W_R}/M_\Delta$  mass ratios. In the right panel, we turn on  $\theta_{\Delta h}$  but fix the  $M_{W_R}/M_\Delta$  mass ratio for each relic curve.

relic curve, there is also an upper bound on  $\theta_{\Delta h}$  otherwise  $\Delta$  would decay too fast.

To justify the use of Eq. (3.10), we must verify that  $\Delta$  decouples from the rest of the plasma while it was still ultra-relativistic. First of all, at temperatures around the LR symmetry breaking scale,  $\Delta$  is in thermal equilibrium with heavy particles that receive their mass from  $v_\Delta$ , which are  $N_{2,3}$  and  $W_R, Z'$ . When the temperature of the universe falls around the  $M_\Delta$ , the  $N_{2,3}$  and  $W_R, Z'$  particles already decouple from the thermal plasma because they are much heavier. The remaining processes to consider are similar to those in FIG. 9. Among them, the process  $\Delta \leftrightarrow \gamma\gamma$  is suppressed by the heavy  $W_R$  mass and remains decoupled until the temperature of the universe cools down to (set by  $\Gamma_{\Delta \leftrightarrow \gamma\gamma} = H$ )

$$T \sim 10^9 \text{ GeV} \left( \frac{M_\Delta}{10^{13} \text{ GeV}} \right)^{1/2} \left( \frac{10^3}{M_{W_R}/M_\Delta} \right). \quad (4.15)$$

This temperature is well below  $M_\Delta$ , thus the inverse decay will be Boltzmann suppressed and never reach equilibrium. As discussed in Eq. (4.14), the other processes  $\Delta \leftrightarrow N_1 N_1$  and  $\Delta \leftrightarrow 4q$  have rates much smaller than  $\Delta \leftrightarrow \gamma\gamma$  and cannot keep  $\Delta$  thermalized either.

Therefore, the decoupling of  $\Delta$  must occur at a temperature between  $M_{W_R}$  and  $M_\Delta$ . The particle mass spectrum considered for the  $\Delta$ -dilution mechanism is indeed compatible with the assumption that  $\Delta$  freezes out relativistically.

## V. CONCLUSION AND OUTLOOK

In this work, we explore the entropy dilution mechanism for dark matter relic density in the minimal LRSM that also addresses the origin of neutrino mass. In this model, the lightest right-handed neutrino ( $N_1$ ) is the sole dark matter candidate and its mass must be below the QCD scale in order to stay cosmologically stable. We first emphasize that  $N_1$  always decouples relativistically from the right-handed current interactions and an entropy release afterwards must happen for producing the observed dark matter relic abundance in the universe. This requires the presence of a “long-lived” diluting particle which comes to dominate the energy content of the universe as a matter component, before decaying away mainly into SM particles. One of the heavier right-handed neutrinos ( $N_2$ ) or the Higgs boson from spontaneous  $SU(2)_R \times U(1)_{B-L}$  gauge symmetry breaking ( $\Delta$ ) can play the role of the diluting particle.

Our original contribution here is a new opportunity of such a mechanism in cosmology. The matter power spectrum for the large scale structure of the universe is sensitive to the diluting particle’s partial decay model into dark matter. When produced this way, dark matter can remain relativistic until the onset of recombination and suppress the primordial matter density perturbations. Through a detailed analysis, we derive an upper bound on such a decay branching ratio to be less than  $\sim 1\%$ , using the existing SDSS data. Such a large scale structure constraint is generic and can be applied to various dark matter models that require an entropy dilution mechanism. In the context of LRSM, the decay of  $N_2$  into  $N_1$  can happen via right-handed charged-current interaction (mediated by the  $W_R^\pm$  gauge boson) and the decay of  $\Delta$  into  $N_1$  is tied to dark matter mass generation. Therefore, the large scale structure constraint plays a crucial role in determining the viable parameter space for the dark matter relic density. We carry out an anatomy of possible dark matter dilution scenarios in the left-right symmetric model:

- In the scenario of  $N_2$  dilution, we point out that the decays of  $N_2$  cannot be dominated by the right-handed currents, otherwise the  $N_2 \rightarrow N_1$  branching ratio is too high

( $\gtrsim 10\%$ ). Thus, additional decay modes must be present due to a  $N_2$ -light-neutrino mixing or  $W - W_R$  gauge boson mixing. In both cases, we find that the mass scale of the  $W_R$  boson must be rather high, above the PeV scale. On the other hand, the dilutor  $N_2$  can have a mass as low as the weak scale. We also derive the mono-chromatic  $X$ -ray constraint on dark matter  $N_1$  from  $W - W_R$  mixing which further narrows down the viable mass range of  $N_1$  to a mass window of  $6.5 - 30$  keV.

- The possibility of  $\Delta$  dilution is original to this work. This scenario requires  $\Delta$  to be lighter than the right-handed gauge bosons and neutrinos (except for  $N_1$ ). We find the  $\Delta \rightarrow \gamma\gamma$  mode to be the most useful for suppressing the  $\Delta \rightarrow N_1 N_1$  decay and passing the strong large scale structure constraint. The corresponding mass scales of  $\Delta$  and  $W_R$  need to be very high, close to the GUT scale. Because of this, the  $W$ - $W_R$  mixing contribution to  $N_1$  dark matter radiative decay is negligible. The  $N_1 \rightarrow \nu\gamma$  decay will only proceed via its mixing with light active neutrinos, as is the case of a regular sterile neutrino.

Based on the above results, we point out the following opportunities of diluted dark matter in the light of the upcoming experimental efforts:

- The primordial dark matter power spectrum will be more precisely measured by the upcoming large scale galaxy surveys, including Euclid and Rubin LSST [106, 107]. Future high-redshift surveys such as MegaMapper and PUMA have the promise to extend the precision measurement up to wave number  $k \sim 0.9 h/\text{Mpc}$  [108]. A discovery of suppressed matter power spectrum, starting from  $k \gtrsim 0.03 h/\text{Mpc}$ , will serve as a smoking-gun evidence for dark matter entropy dilution mechanism in the early universe with a nonzero dilutor to dark matter decay branching ratio.
- Related to the thermal dark matter population that gets diluted, future experimental facilities exploring the small scale structure of the universe will be instrumental as well. Observations of low mass dark matter halos and the lensing of cosmic microwave background may allow the discovery and measurements of the dark matter mass, if it lies not far above the current lower bound ( $\sim 6.5$  keV) [109, 110].
- Future experiments including ATHENA and XRISM [99–101] will search for mono-chromatic  $X$  ray emission from the radiative decay of  $N_1$  dark matter in the Milky

Way and nearby galaxies. A positive measurement will be useful as another input to discriminate between the various dark matter dilution scenarios and neutrino mass generation mechanisms in the LRSM, and map out the favored parameter space.

On the theory side, a follow-up exercise will be to calculate the evolution of primordial matter density perturbations by taking into account the non-linear terms in the Boltzmann equations, which start to become non-negligible (bringing in corrections of percent level or higher) for wave numbers  $k \gtrsim 0.2 h/\text{Mpc}$  and observations made at redshift  $z \approx 0$  [86, 111, 112]. Because the hot dark matter component from dilutor decay acts to suppress the perturbations, we expect the non-linear effect to be smaller than the case of regular cold/warm dark matter. Nonetheless, a more careful analysis is warranted and can serve as a useful tool for discovering this piece of new physics in the upcoming precision cosmology era.

## ACKNOWLEDGEMENTS

We thank Weiyi Deng, Diego Redigolo, Filippo Sala and Katelin Schutz for useful discussions and correspondence. MN is supported by the Slovenian Research Agency under the research core funding No. P1-0035 and in part by the research grants J1-3013, N1-0253 and J1-4389. YZ is supported by a Subatomic Physics Discovery Grant (individual) from the Natural Sciences and Engineering Research Council of Canada, and by the Canada First Research Excellence Fund through the Arthur B. McDonald Canadian Astroparticle Physics Research Institute.

## Appendix A: Radiative $N_1$ decay via $W - W_R$ mixing

The radiative decay of dark matter to a monochromatic photon  $N_1 \rightarrow \nu\gamma$  gives a very stringent constraint on its couplings from the X-ray spectra measurements, shown in Fig. 8. Here we provide some details on the calculation of the rate in Eq. (4.12), which has new sources within the LRSM. There are two possible contributions, one from the Dirac mixing of  $N_1$  with  $\nu$ , which is well known and the same as for the sterile neutrinos. In the presence of gauge boson mixing  $\xi_{LR}$ , another amplitude is present, coming from the SM-like  $W$  having



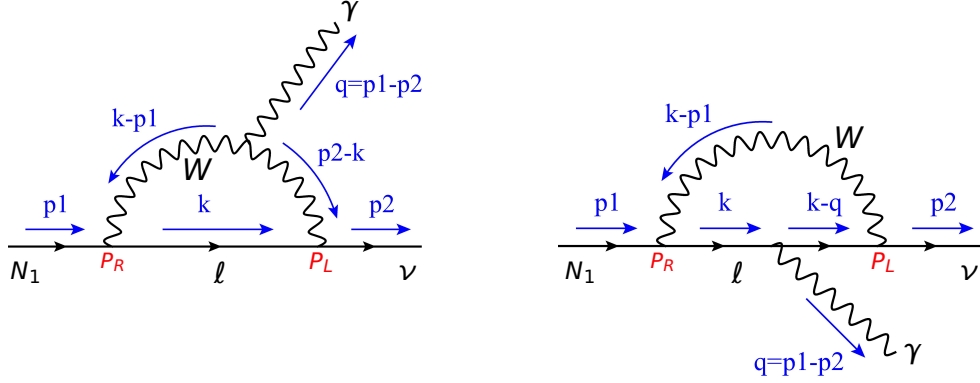


FIG. 11. Feynman diagrams for  $N_1$  radiative decay via  $W - W_R$  mixing in the LRSM. The  $W$ - $N_1$ - $\ell$  vertex labelled by  $\mathbb{P}_R$  is induced by the  $W$ - $W_R$  mixing and the corresponding Feynman rule is obtained from the second term in Eq. (A1).

a coupling to the right-handed charged current. In the small  $\xi_{LR}$  limit we have

$$\mathcal{L}_{CC} \simeq \frac{g}{\sqrt{2}} \left[ \bar{\nu}_\ell \gamma^\mu \mathbb{P}_L \ell + \xi_{LR} \left( V_{PMNS}^{R\dagger} \right)_{i\ell} \bar{N}_i \gamma^\mu \mathbb{P}_R \ell \right] W_\mu^+ + \text{h.c.}, \quad (\text{A1})$$

where  $V_{PMNS}^{R\dagger}$  is the right-handed PMNS matrix introduced in Eq. (2.4). With this coupling turned on, there are two new diagrams contributing to radiative  $N_1$  decay, and their topologies are shown in Fig. 11.

The  $N_1 \rightarrow \nu\gamma$  decay always occurs via the dimension-5 effective operator

$$\mathcal{L}_{\text{eff}} = C \bar{\nu} \sigma_{\mu\nu} \mathbb{P}_R N_1 F^{\mu\nu} + \text{h.c.}, \quad (\text{A2})$$

where  $C$  is the Wilson coefficient, to be determined next, and  $\sigma_{\mu\nu} \equiv \frac{i}{2} [\gamma^\mu, \gamma^\nu]$ . The chiral projection operator in front of the  $N_1$  field must be  $\mathbb{P}_R = (1 + \gamma_5)/2$ . The corresponding decay amplitude for  $N_1(p_1) \rightarrow \nu(p_2)\gamma(q)$  is

$$i\mathcal{M} = -iC \bar{u}_\nu(p_2, s_2) (q \not{\varepsilon}^* - \varepsilon^* \not{q}) \mathbb{P}_R u_N(p_1, s_1). \quad (\text{A3})$$

where  $\varepsilon_\mu^*$  is the photon polarization vector and  $q \cdot \varepsilon^*(q) = 0$  for an on-shell transverse photon. The partial decay rate of  $N_1 \rightarrow \nu\gamma$  is

$$\Gamma_{N_1 \rightarrow \nu\gamma} = \frac{1}{4\pi} |C|^2 m_{N_1}^3. \quad (\text{A4})$$

For a Majorana  $N_1$ , it can also decay into  $\bar{\nu}\gamma$  with the same partial rate.

With the momentum assignments shown in Fig. 11, the first diagram has an amplitude

$$\begin{aligned}
i\mathcal{M}_1 = & -\frac{eg^2}{2}\xi_{\text{LR}} \sum_{\ell} (V_{\text{PMNS}}^{R\dagger})_{1\ell} m_{\ell} \int \frac{d^4k}{(2\pi)^4} \frac{1}{(k^2 - m_{\ell}^2)[(k - p_1)^2 - M_W^2][(p_2 - k)^2 - M_W^2]} \\
& \times \left\{ (2k - p_1 - p_2) \cdot \varepsilon^* \bar{u}_{\nu}(p_2, s_2) \gamma^{\mu} \gamma_{\mu} \mathbb{P}_R u_N(p_1, s_1) \right. \\
& \left. + \bar{u}_{\nu}(p_2, s_2) \not{\varepsilon}^* (\not{p}_2 - \not{K} - \not{q}) \mathbb{P}_R u_N(p_1, s_1) + \bar{u}_{\nu}(p_2, s_2) (\not{q} - \not{K} + \not{p}_1) \not{\varepsilon}^* \mathbb{P}_R u_N(p_1, s_1) \right\}, \tag{A5}
\end{aligned}$$

where we have dropped terms that are suppressed by additional powers of  $1/M_W$ . For the  $\gamma$  matrices between the fermion spinors, we are interested in the structure  $\not{q}\not{\varepsilon}^* - \not{\varepsilon}^*\not{q}$ , as in Eq. (A3). This immediately implies that the first term in  $\{\}$  does not contribute. In addition, because the external fermions already have the correct chirality, we can drop the chirality-flipping terms (upon equation of motion) such as  $\not{p}_1$  acting on  $u_N(p_1, s_1)$  and  $\not{p}_2$  acting on  $\bar{u}_{\nu}(p_2, s_2)$ . This allows us to reduce the  $\{\}$  bracket in Eq. (A5) into

$$\left\{ \right\} \rightarrow \bar{u}(p_2, s_2) (\not{\varepsilon}^* (-\not{K} - 2\not{q}) + (2\not{q} - \not{K}) \not{\varepsilon}^*) \mathbb{P}_R u(p_1, s_1). \tag{A6}$$

After completing the  $k$  integral, the remaining relevant term is

$$i\mathcal{M}_1 = i \frac{eg^2}{16\pi^2} \xi_{\text{LR}} \sum_{\ell} (V_{\text{PMNS}}^{R\dagger})_{1\ell} \frac{m_{\ell}}{M_W^2} \bar{u}(p_2, s_2) (\not{q}\not{\varepsilon}^* - \not{\varepsilon}^*\not{q}) \mathbb{P}_R u(p_1, s_1). \tag{A7}$$

The second diagram of Fig. 11 has an amplitude

$$\begin{aligned}
i\mathcal{M}_2 = & -\frac{eg^2}{2}\xi_{\text{LR}} \sum_{\ell} (V_{\text{PMNS}}^{R\dagger})_{1\ell} m_{\ell} \int \frac{d^4k}{(2\pi)^4} \frac{1}{(k^2 - m_{\ell}^2)[(k - q)^2 - m_{\ell}^2][(k - p_1)^2 - M_W^2]} \\
& \times \left\{ \bar{u}_{\nu}(p_2, s_2) \gamma^{\mu} \not{\varepsilon}^* \not{K} \gamma_{\mu} \mathbb{P}_R u_N(p_1, s_1) + \bar{u}_{\nu}(p_2, s_2) \gamma^{\mu} (\not{K} - \not{q}) \not{\varepsilon}^* \gamma_{\mu} \mathbb{P}_R u_N(p_1, s_1) \right\}. \tag{A8}
\end{aligned}$$

Using the identity  $\gamma^{\mu} \gamma^{\beta} \gamma^{\rho} \gamma_{\mu} = 4g^{\beta\rho}$ , all the  $\gamma$  matrices between  $\bar{u}_{\nu}(p_2, s_2)$  and  $u_N(p_1, s_1)$  are gone. Thus, we conclude that this diagram does not contribute to the  $N_1 \rightarrow \nu\gamma$  decay.

Comparing Eqs. (A3) and (A7), we get

$$C = -\frac{eG_F \xi_{\text{LR}} \sum_{\ell} (V_{\text{PMNS}}^{R\dagger})_{1\ell} m_{\ell}}{2\sqrt{2}\pi^2}. \tag{A9}$$

The corresponding  $N_1$  radiative decay rate is

$$\Gamma_{N_1 \rightarrow \nu\gamma} = \frac{\alpha \xi_{\text{LR}}^2}{8\pi^4} G_F^2 m_{N_1}^3 \sum_{\ell} |(V_{\text{PMNS}}^R)_{\ell 1}|^2 m_{\ell}^2. \tag{A10}$$

This is how we get Eq. (4.12) in the main text.

---

- [1] S. Dodelson and L. M. Widrow, *Phys. Rev. Lett.* **72**, 17 (1994), [arXiv:hep-ph/9303287](#).
- [2] X.-D. Shi and G. M. Fuller, *Phys. Rev. Lett.* **82**, 2832 (1999), [arXiv:astro-ph/9810076](#).
- [3] E. O. Nadler *et al.* (DES), *Phys. Rev. Lett.* **126**, 091101 (2021), [arXiv:2008.00022 \[astro-ph.CO\]](#).
- [4] K. N. Abazajian, *Phys. Rept.* **711-712**, 1 (2017), [arXiv:1705.01837 \[hep-ph\]](#).
- [5] A. De Gouvêa, M. Sen, W. Tangarife, and Y. Zhang, *Phys. Rev. Lett.* **124**, 081802 (2020), [arXiv:1910.04901 \[hep-ph\]](#).
- [6] K. J. Kelly, M. Sen, W. Tangarife, and Y. Zhang, *Phys. Rev. D* **101**, 115031 (2020), [arXiv:2005.03681 \[hep-ph\]](#).
- [7] K. J. Kelly, M. Sen, and Y. Zhang, *Phys. Rev. Lett.* **127**, 041101 (2021), [arXiv:2011.02487 \[hep-ph\]](#).
- [8] R. An, V. Gluscevic, E. O. Nadler, and Y. Zhang, *Astrophys. J. Lett.* **954**, L18 (2023), [arXiv:2301.08299 \[astro-ph.CO\]](#).
- [9] J. C. Pati and A. Salam, *Phys. Rev.* **D10**, 275 (1974), [Erratum: *Phys. Rev.*D11,703(1975)].
- [10] H. Fritzsch and P. Minkowski, *Annals Phys.* **93**, 193 (1975).
- [11] R. N. Mohapatra and G. Senjanović, *Phys. Rev. Lett.* **44**, 912 (1980), [,231(1979)].
- [12] R. N. Mohapatra and J. C. Pati, *Phys. Rev.* **D11**, 2558 (1975).
- [13] G. Senjanović and R. N. Mohapatra, *Phys. Rev.* **D12**, 1502 (1975).
- [14] G. Senjanović, *Nucl. Phys.* **B153**, 334 (1979).
- [15] M. Nemevšek, G. Senjanović, and V. Tello, *Phys. Rev. Lett.* **110**, 151802 (2013), [arXiv:1211.2837 \[hep-ph\]](#).
- [16] W.-Y. Keung and G. Senjanović, *Phys. Rev. Lett.* **50**, 1427 (1983).
- [17] M. Nemevsek, F. Nesti, G. Senjanovic, and Y. Zhang, *Phys. Rev. D* **83**, 115014 (2011), [arXiv:1103.1627 \[hep-ph\]](#).
- [18] R. N. Mohapatra and G. Senjanović, *Phys. Rev.* **D23**, 165 (1981).
- [19] V. Tello, M. Nemevšek, F. Nesti, G. Senjanović, and F. Vissani, *Phys. Rev. Lett.* **106**, 151801 (2011), [arXiv:1011.3522 \[hep-ph\]](#).
- [20] V. Cirigliano, A. Kurylov, M. J. Ramsey-Musolf, and P. Vogel, *Phys. Rev. D* **70**, 075007

- (2004), [arXiv:hep-ph/0404233](#).
- [21] M. Nemevsek, F. Nesti, G. Senjanovic, and V. Tello, [arXiv \(2011\)](#), [arXiv:1112.3061 \[hep-ph\]](#).
- [22] R. N. Mohapatra and X. Zhang, [Phys. Rev. D](#) **46**, 5331 (1992).
- [23] A. S. Joshipura, E. A. Paschos, and W. Rodejohann, [Nucl. Phys. B](#) **611**, 227 (2001), [arXiv:hep-ph/0104228](#).
- [24] J.-M. Frere, T. Hambye, and G. Vertongen, [JHEP](#) **01** (051), [arXiv:0806.0841 \[hep-ph\]](#).
- [25] P. S. Bhupal Dev, C.-H. Lee, and R. N. Mohapatra, [Phys. Rev. D](#) **90**, 095012 (2014), [arXiv:1408.2820 \[hep-ph\]](#).
- [26] F. Bezrukov, H. Hettmansperger, and M. Lindner, [Phys. Rev. D](#) **81**, 085032 (2010), [arXiv:0912.4415 \[hep-ph\]](#).
- [27] S. Tremaine and J. Gunn, [Phys. Rev. Lett.](#) **42**, 407 (1979).
- [28] A. Boyarsky, O. Ruchayskiy, and D. Iakubovskiy, [JCAP](#) **03** (005), [arXiv:0808.3902 \[hep-ph\]](#).
- [29] M. Viel, G. D. Becker, J. S. Bolton, and M. G. Haehnelt, [Phys. Rev. D](#) **88**, 043502 (2013), [arXiv:1306.2314 \[astro-ph.CO\]](#).
- [30] V. Iršič *et al.*, [Phys. Rev. D](#) **96**, 023522 (2017), [arXiv:1702.01764 \[astro-ph.CO\]](#).
- [31] D. Gilman, S. Birrer, A. Nierenberg, T. Treu, X. Du, and A. Benson, [Mon. Not. Roy. Astron. Soc.](#) **491**, 6077 (2020), [arXiv:1908.06983 \[astro-ph.CO\]](#).
- [32] J.-W. Hsueh, W. Enzi, S. Vegetti, M. Auger, C. D. Fassnacht, G. Despali, L. V. E. Koopmans, and J. P. McKean, [Mon. Not. Roy. Astron. Soc.](#) **492**, 3047 (2020), [arXiv:1905.04182 \[astro-ph.CO\]](#).
- [33] W. Enzi *et al.*, [Mon. Not. Roy. Astron. Soc.](#) **506**, 5848 (2021), [arXiv:2010.13802 \[astro-ph.CO\]](#).
- [34] E. O. Nadler, S. Birrer, D. Gilman, R. H. Wechsler, X. Du, A. Benson, A. M. Nierenberg, and T. Treu, [Astrophys. J.](#) **917**, 7 (2021), [arXiv:2101.07810 \[astro-ph.CO\]](#).
- [35] R. J. Scherrer and M. S. Turner, [Phys. Rev. D](#) **31**, 681 (1985).
- [36] M. Nemevšek, G. Senjanović, and Y. Zhang, [JCAP](#) **07** (006), [arXiv:1205.0844 \[hep-ph\]](#).
- [37] M. Nemevšek and Y. Zhang, [Phys. Rev. Lett.](#) **130**, 121002 (2023), [arXiv:2206.11293 \[hep-ph\]](#).
- [38] T. Moroi and L. Randall, [Nucl. Phys. B](#) **570**, 455 (2000), [arXiv:hep-ph/9906527](#).
- [39] E. A. Baltz and H. Murayama, [JHEP](#) **05** (067), [arXiv:astro-ph/0108172](#).
- [40] T. Asaka, M. Shaposhnikov, and A. Kusenko, [Phys. Lett. B](#) **638**, 401 (2006), [arXiv:hep-ph/0602150](#).
- [41] J. Hasenkamp and J. Kersten, [Phys. Rev. D](#) **82**, 115029 (2010), [arXiv:1008.1740 \[hep-ph\]](#).

- [42] G. Arcadi and P. Ullio, *Phys. Rev. D* **84**, 043520 (2011), [arXiv:1104.3591 \[hep-ph\]](#).
- [43] Y. Zhang, *JCAP* **05** (008), [arXiv:1502.06983 \[hep-ph\]](#).
- [44] A. V. Patwardhan, G. M. Fuller, C. T. Kishimoto, and A. Kusenko, *Phys. Rev. D* **92**, 103509 (2015), [arXiv:1507.01977 \[astro-ph.CO\]](#).
- [45] Z. Chacko, N. Craig, P. J. Fox, and R. Harnik, *JHEP* **07** (023), [arXiv:1611.07975 \[hep-ph\]](#).
- [46] M. Cirelli, P. Panci, K. Petraki, F. Sala, and M. Taoso, *JCAP* **05** (036), [arXiv:1612.07295 \[hep-ph\]](#).
- [47] A. Soni, H. Xiao, and Y. Zhang, *Phys. Rev. D* **96**, 083514 (2017), [arXiv:1704.02347 \[hep-ph\]](#).
- [48] R. Contino, A. Mitridate, A. Podo, and M. Redi, *JHEP* **02** (187), [arXiv:1811.06975 \[hep-ph\]](#).
- [49] J. A. Evans, A. Ghalsasi, S. Gori, M. Tamaro, and J. Zupan, *JHEP* **02** (151), [arXiv:1910.06319 \[hep-ph\]](#).
- [50] C. Cosme, M. Dutra, T. Ma, Y. Wu, and L. Yang, *JHEP* **03** (026), [arXiv:2003.01723 \[hep-ph\]](#).
- [51] J. A. Dror, D. Dunsky, L. J. Hall, and K. Harigaya, *JHEP* **07** (168), [arXiv:2004.09511 \[hep-ph\]](#).
- [52] P. Chanda and J. Unwin, *JCAP* **06** (032), [arXiv:2102.02313 \[hep-ph\]](#).
- [53] P. Asadi, T. R. Slatyer, and J. Smirnov, *arXiv* (2021), [arXiv:2111.11444 \[hep-ph\]](#).
- [54] S. Baumholzer and P. Schwaller, *JCAP* **06** (06), 013, [arXiv:2112.03993 \[hep-ph\]](#).
- [55] K. Bleau, J. Bramante, and C. Cappiello, *arXiv* (2023), [arXiv:2309.06482 \[hep-ph\]](#).
- [56] J. Basecq, *SCALAR SECTOR IN  $SU(2)$ - $L \times SU(2)$ - $R \times U(1)$ -( $B$ - $L$ ) MODELS*, Other thesis, Carnegie Mellon U. (1986).
- [57] J. F. Gunion, J. Grifols, A. Mendez, B. Kayser, and F. I. Olness, *Phys. Rev. D* **40**, 1546 (1989).
- [58] K. Kiers, J. Kolb, J. Lee, A. Soni, and G.-H. Wu, *Phys. Rev. D* **66**, 095002 (2002), [arXiv:hep-ph/0205082](#).
- [59] N. G. Deshpande, J. F. Gunion, B. Kayser, and F. I. Olness, *Phys. Rev. D* **44**, 837 (1991).
- [60] P. Duka, J. Gluza, and M. Zralek, *Annals Phys.* **280**, 336 (2000), [arXiv:hep-ph/9910279](#).
- [61] O. Khasanov and G. Perez, *Phys. Rev. D* **65**, 053007 (2002), [arXiv:hep-ph/0108176](#).
- [62] W. Dekens and D. Boer, *Nucl. Phys. B* **889**, 727 (2014), [arXiv:1409.4052 \[hep-ph\]](#).
- [63] G. Bambhaniya, J. Chakraborty, J. Gluza, T. Jelinski, and R. Szafron, *Phys. Rev. D* **92**, 015016 (2015), [arXiv:1504.03999 \[hep-ph\]](#).
- [64] P. S. B. Dev, R. N. Mohapatra, and Y. Zhang, *JHEP* (05), 174, [arXiv:1602.05947 \[hep-ph\]](#).

- [65] A. Maiezza, M. Nemevšek, and F. Nesti, *Phys. Rev. D* **94**, 035008 (2016), [arXiv:1603.00360 \[hep-ph\]](#).
- [66] P. S. Bhupal Dev, R. N. Mohapatra, W. Rodejohann, and X.-J. Xu, *JHEP* (02), 154, [arXiv:1811.06869 \[hep-ph\]](#).
- [67] V. Brdar, L. Graf, A. J. Helmboldt, and X.-J. Xu, *JCAP* **12** (027), [arXiv:1909.02018 \[hep-ph\]](#).
- [68] Y. Zhang, H. An, X. Ji, and R. N. Mohapatra, *Nucl. Phys.* **B802**, 247 (2008), [arXiv:0712.4218 \[hep-ph\]](#).
- [69] Y. Zhang, H. An, X. Ji, and R. N. Mohapatra, *Phys. Rev. D* **76**, 091301 (2007), [arXiv:0704.1662 \[hep-ph\]](#).
- [70] A. Maiezza, M. Nemevšek, F. Nesti, and G. Senjanović, *Phys. Rev. D* **82**, 055022 (2010), [arXiv:1005.5160 \[hep-ph\]](#).
- [71] G. Senjanović and V. Tello, *Phys. Rev. Lett.* **114**, 071801 (2015), [arXiv:1408.3835 \[hep-ph\]](#).
- [72] G. Senjanović and V. Tello, *Phys. Rev. D* **94**, 095023 (2016), [arXiv:1502.05704 \[hep-ph\]](#).
- [73] A. Maiezza and M. Nemevšek, *Phys. Rev.* **D90**, 095002 (2014), [arXiv:1407.3678 \[hep-ph\]](#).
- [74] S. Bertolini, A. Maiezza, and F. Nesti, *Phys. Rev. D* **101**, 035036 (2020), [arXiv:1911.09472 \[hep-ph\]](#).
- [75] S. Bertolini, L. Di Luzio, and F. Nesti, *Phys. Rev. Lett.* **126**, 081801 (2021), [arXiv:2006.12508 \[hep-ph\]](#).
- [76] S. Weinberg, *Phys. Rev. Lett.* **36**, 294 (1976).
- [77] A. D. Linde, *JETP Lett.* **23**, 64 (1976).
- [78] J. Basecq and D. Wyler, *Phys. Rev. D* **39**, 870 (1989).
- [79] M. Nemevšek, F. Nesti, and J. C. Vasquez, *JHEP* **04** (114), [arXiv:1612.06840 \[hep-ph\]](#).
- [80] M. Nemevšek, F. Nesti, and G. Popara, *Phys. Rev. D* **97**, 115018 (2018), [arXiv:1801.05813 \[hep-ph\]](#).
- [81] M. Nemevšek and F. Nesti, *PRD* (2023), [arXiv:2306.12104 \[hep-ph\]](#).
- [82] P. A. Zyla *et al.* (Particle Data Group), *PTEP* **2020**, 083C01 (2020).
- [83] N. Aghanim *et al.* (Planck), *Astron. Astrophys.* **641**, A6 (2020), [arXiv:1807.06209 \[astro-ph.CO\]](#).
- [84] J. Lesgourgues, *arXiv* (2011), [arXiv:1104.2932 \[astro-ph.IM\]](#).
- [85] D. Blas, J. Lesgourgues, and T. Tram, *JCAP* **07** (034), [arXiv:1104.2933 \[astro-ph.CO\]](#).
- [86] J. Lesgourgues and T. Tram, *JCAP* **09** (032), [arXiv:1104.2935 \[astro-ph.CO\]](#).

- [87] B. A. Reid *et al.*, *Mon. Not. Roy. Astron. Soc.* **404**, 60 (2010), [arXiv:0907.1659 \[astro-ph.CO\]](#).
- [88] K.-G. Lee *et al.*, *Astron. J.* **145**, 69 (2013), [arXiv:1211.5146 \[astro-ph.CO\]](#).
- [89] F. D’Eramo and A. Lenoci, *JCAP* **10** (045), [arXiv:2012.01446 \[hep-ph\]](#).
- [90] Q. Decant, J. Heisig, D. C. Hooper, and L. Lopez-Honorez, *JCAP* **03** (03), 041, [arXiv:2111.09321 \[astro-ph.CO\]](#).
- [91] J. A. Casas and A. Ibarra, *Nucl. Phys. B* **618**, 171 (2001), [arXiv:hep-ph/0103065](#).
- [92] A. Davidson, *Phys. Rev. D* **20**, 776 (1979).
- [93] R. N. Mohapatra and R. E. Marshak, *Phys. Rev. Lett.* **44**, 1316 (1980), [Erratum: *Phys.Rev.Lett.* 44, 1643 (1980)].
- [94] R. Shrock, *Phys. Rev. D* **9**, 743 (1974).
- [95] P. B. Pal and L. Wolfenstein, *Phys. Rev. D* **25**, 766 (1982).
- [96] A. Boyarsky, D. Malyshev, A. Neronov, and O. Ruchayskiy, *Mon. Not. Roy. Astron. Soc.* **387**, 1345 (2008), [arXiv:0710.4922 \[astro-ph\]](#).
- [97] A. Merle and V. Niro, *Phys. Rev. D* **88**, 113004 (2013), [arXiv:1302.2032 \[hep-ph\]](#).
- [98] K. C. Y. Ng, B. M. Roach, K. Perez, J. F. Beacom, S. Horiuchi, R. Krivonos, and D. R. Wik, *Phys. Rev. D* **99**, 083005 (2019), [arXiv:1901.01262 \[astro-ph.HE\]](#).
- [99] A. Neronov and D. Malyshev, *Phys. Rev. D* **93**, 063518 (2016), [arXiv:1509.02758 \[astro-ph.HE\]](#).
- [100] XRISM Science Team, [arXiv 10.48550/arXiv.2003.04962](#) (2020), [arXiv:2003.04962 \[astro-ph.HE\]](#).
- [101] C. Dessert, O. Ning, N. L. Rodd, and B. R. Safdi, [arXiv](#) (2023), [arXiv:2305.17160 \[astro-ph.CO\]](#).
- [102] S. Colombi, S. Dodelson, and L. M. Widrow, *Astrophys. J.* **458**, 1 (1996), [arXiv:astro-ph/9505029](#).
- [103] M. Viel, J. Lesgourgues, M. G. Haehnelt, S. Matarrese, and A. Riotto, *Phys. Rev. D* **71**, 063534 (2005), [arXiv:astro-ph/0501562](#).
- [104] R. N. Mohapatra, *Adv. Ser. Direct. High Energy Phys.* **3**, 384 (1989).
- [105] A. Djouadi, *Phys. Rept.* **457**, 1 (2008), [arXiv:hep-ph/0503172](#).
- [106] A. Ealet, *Cosmology with the EUCLID satellite: Mapping the large structures of the Universe Probing dark energy* (2017).
- [107] S. Ferraro, N. Sailer, A. Slosar, and M. White, [arXiv](#) (2022), [arXiv:2203.07506 \[astro-ph.CO\]](#).

- [108] N. Sailer, E. Castorina, S. Ferraro, and M. White, *JCAP* **2112** (12), 049, published in *JCAP*, [arXiv:2106.09713](#).
- [109] S. Chakrabarti *et al.*, in *Snowmass 2021* (2022) [arXiv:2203.06200](#) [astro-ph.CO].
- [110] A. Drlica-Wagner *et al.*, *arXiv* (2022), [arXiv:2209.08215](#) [hep-ph].
- [111] V. Junk and E. Komatsu, *Phys. Rev. D* **85**, 123524 (2012), [arXiv:1204.3789](#) [astro-ph.CO].
- [112] J. J. M. Carrasco, S. Foreman, D. Green, and L. Senatore, *JCAP* **07** (057), [arXiv:1310.0464](#) [astro-ph.CO].